Acta Mech 224, 1823–1848 (2013)
DOI 10.1007/s00707-013-0840-3

P. M. Adler · A. E. Malevich · V. V. Mityushev

Nonlinear correction to Darcy's law for channels with wavy walls

Received: 6 November 2012 / Revised: 13 February 2013 / Published online: 26 March 2013

Abstract For low Reynolds numbers $\mathcal{R}$, the flow of a viscous fluid through a channel is described by the well-known Darcy's law which corresponds to a linear relation between the pressure gradient $\overline{\nabla p}$ and the average velocity $\overline{u}$. When the channel is not straight and when the Reynolds number is not negligible, additional terms appear in this relation. Some previous authors investigated the first three coefficients in the expansion of $|\overline{\nabla p}|$ in the powers of $\overline{u}$ and they showed that the coefficient of $\overline{u}^2$ vanishes for moderate $\mathcal{R}$. Other authors demonstrated that this coefficient can be non-zero. This question is addressed and solved. It is demonstrated that both cases occur; Forchheimer's law has a cubic correction for small $\mathcal{R}$ and a quadratic one for large $\mathcal{R}$. Two analytical–numerical algorithms are constructed to prove this property. These algorithms are applied to the Navier–Stokes equations in three-dimensional channels enclosed by two wavy walls whose amplitude is proportional to $b\varepsilon$, where $2b$ is the mean clearance of the channels and ε is a small dimensionless parameter. The first algorithm is applied for small $\mathcal{R}$ by representing the velocity and the pressure in terms of a double Taylor series in $\mathcal{R}$ and ε. The accuracy $O(\mathcal{R}^2)$ and $O(\varepsilon^6)$ following Padé approximations yield analytical approximate formulae for Forchheimer's law. The first algorithm is applied to symmetric channels on the theoretical level (all terms on $\mathcal{R}$ and ε are taken into account) to show that $|\overline{\nabla p}|$ is an odd function of $\overline{u}$. This observation yields, in particular, a cubic correction to Darcy's law. Numerical examples for non-symmetrical channels yield the same cubic correction. The second algorithm is based on the analytical–numerical solution to the Navier–Stokes equations for arbitrary $\mathcal{R}$ up to $O(\varepsilon^3)$. This algorithm yields, in particular, a quadratic correction to Darcy's law for higher $\mathcal{R}$.

1 Introduction

The present paper is devoted to flow of a viscous fluid through a channel. The classical Poiseuille flow in the channel bounded by two parallel planes separated by a distance $2b$ is generated by an average pressure gradient $\overline{\nabla p}$. The flow profile is parabolic when the viscous forces are dominant over inertial forces. It yields

P. M. Adler (✉)
Sisyphe, Université P.-M. Curie Paris VI, tour 46, place Jussieu,
75252 Paris Cedex 05, France
Tel.: +33-1-44272428
Fax: +33-1-44274588
E-mail: pierre.adler@upmc.fr

A. E. Malevich
Department of Mechanics and Mathematics, BSU, pr. Nezavisimosti 4, 220050 Minsk, Belarus

V. V. Mityushev
Department of Computer Sciences and Computer Methods, Pedagogical University,
ul. Podchorazych 2, 30-084 Krakow, Poland

the well-known Darcy's law, i.e., a linear dependence between $|\overline{\nabla p}|$ and the average component of the velocity $\overline{u}$ along the pressure gradient [1]

$$|\overline{\nabla p}| = \frac{\mu}{K}\overline{u}. \tag{1}$$

When inertial forces are dominant, (1) is not valid anymore and it becomes nonlinear.

The structure of the nonlinear Darcy's law for general porous media has attracted the attention of many scientists because it is of fundamental interest since it illustrates the mechanism of viscous flow under different geometrical and physical conditions. In 1901, Forchheimer [2] proposed corrections to Darcy's law in the form

$$|\overline{\nabla p}| = \frac{\mu}{K}\overline{u} + b\overline{u}^m \tag{2}$$

with m close to 2 and

$$|\overline{\nabla p}| = \frac{\mu}{K}\overline{u} + b\overline{u}^2 + c\overline{u}^3. \tag{3}$$

In Petroleum Engineering, (3) is frequently used with an appropriate value of b and $c = 0$:

$$|\overline{\nabla p}| = \frac{\mu}{K}\overline{u} + b\overline{u}^2. \tag{4}$$

The coefficients b and c from (3) and their dependence on the velocity were investigated in [4]. Generalized Forchheimer equations (the Brinkman–Forchheimer model, etc.) and influence of the convection were discussed in [4–7]. The recent studies of [3,8–10] showed that (4) should have another form. These authors applied the homogenization theory to the Navier–Stokes equations in a periodic cell of dimension $2L$ in order to determine the general dependence of $|\overline{\nabla p}|$ on $\overline{u}$. The Reynolds number $\mathcal{R}$, which is the ratio between viscous and inertial forces, can be expressed as:

$$\mathcal{R} = \frac{|\overline{\nabla p}| l^3 \rho}{\mu^2} \tag{5}$$

with $\ell = \frac{L}{\pi}$. The relation between $|\overline{\nabla p}|$ and $\overline{u}$ involves the local Reynolds number in the periodic cell. [3,8] found that for homogeneous and isotropic porous media, Eq. (3) is satisfied with $b = 0$ and $c \geq 0$:

$$|\overline{\nabla p}| = \frac{\mu}{K}\overline{u} + c\overline{u}^3. \tag{6}$$

Moreover, [3] considered a two-dimensional corrugated channel for which (6) is verified. It is worth noting that small and moderate Reynolds numbers were considered in [3,8,9]. This implies that the solution of the dimensionless Navier–Stokes equations depends analytically on $\mathcal{R}$. Recently, Balhoff et al [11] applied homogenization and found that there is no quadratic term for $\mathcal{R} \sim 1$. They established that the filtration law in isotropic media can be obtained by solving a series of successive Stokes problems. The first five coefficients of the infinite series were determined for an axisymmetric sinusoidal channel for which the quadratic and the fourth-order terms vanish.

Whitaker [12] applied the method of volume averaging when $\mathcal{R} \sim 1$ and obtained the quadratic equation (4). Chen et al. [13] unlike [3,8,9] showed that the nonlinear correction is quadratic as in (4). Chen et al. [13] used the same homogenization approach as in [3,8,9], but take a different scaling; the small parameter used in homogenization is the ratio between the pore and the macroscopic scales. An example of rotational flow is given in [13], where the average velocity satisfies the quadratic equation (4). However, this example is not suitable for porous media.

High velocity laminar and turbulent flows in porous media (where $\mathcal{R}$ is large) were discussed in [14] by combining homogenization and boundary layer theories; a nonlinear dependence was obtained which is expressed as:

$$|\overline{\nabla p}| = c\overline{u}^{3/2}. \tag{7}$$

In order to obtain corrections to Darcy's law, one has to solve a boundary value problem for the stationary Navier–Stokes equations for curvilinear channels. We apply a method of perturbation in the oscillation ε of the wavy walls [15,16]. Similar methods were also applied in the papers [17–19]. Moreover, Heining et al.

[19] investigated the gravity-driven free surface flow over three-dimensional channels with sinusoidal bottoms by the combination of the asymptotic and finite volume methods. The effects of side walls on the primary instability of a gravity-driven thin liquid film flowing down in an open channel were investigated in [20,21].

In the present paper, an asymptotic analysis in ε is applied to curvilinear three-dimensional channels bounded by walls of the form

$$z = S^{+}(x, y) \equiv b\big[1 + \varepsilon T(x, y)\big], \tag{8}$$

$$z = S^{-}(x, y) \equiv -b\big[1 + \varepsilon B(x, y)\big], \tag{9}$$

where $b\varepsilon$ is the amplitude of the wall oscillations and ε a small dimensionless parameter. Arbitrary profiles $S^{\pm}(x, y)$ which satisfy some natural conditions described below are considered. Two constructive algorithms are proposed to solve the Navier–Stokes equations in three-dimensional channels in order to deduce the dependence

$$|\overline{\nabla p}| = h(\overline{u}). \tag{10}$$

The first algorithm is based on the representation of the velocity and the pressure in terms of a Taylor series near the point $\mathcal{R} = 0$ and it is applied to flows with small $\mathcal{R}$ in channels symmetric with respect to the xz- and yz-planes. It is proved that in this case $h(\overline{u})$ is an odd function. Thus, "the odd law" which includes the cubic law (6) (see also [11]), is rigorously justified for symmetric channels.

Application of the first algorithm in Sect. 3.3 yields the coefficients of (2)–(6) in analytical and numerical forms that exactly show their structure and quantitative contribution. The presented examples for two-dimensional non-symmetric channels show that the quadratic term vanishes. This confirms the conjecture about the cubic equation (6) for general channels for sufficiently small Reynolds numbers.

The second algorithm is similar to the algorithm of [15], where the Couette flow is investigated for arbitrary Reynolds numbers. The considered Poiseuille flow is more complicated than the Couette flow because in the latter case the basic ordinary differential equation was solved in terms of Airy functions [15]. In the present paper, the basic equation (61) cannot be solved analytically. However, an algorithm related to the "shooting method" is worked out and accurate solutions are obtained for $\mathcal{R}$ up to 10^{10}.

It is shown that a correction for large $\mathcal{R}$ contains the power term $\overline{u}^{4/3}$ which should be compared to (7) in [14].

2 Navier–Stokes equations and Forchheimer's law

Let the profiles $S^{\pm}$ be determined by Eqs. (8) and (9) where the functions $T(x, y)$ and $B(x, y)$ are defined in the square $[-L, L] \times [-L, L]$ of the plane XOY. T and B are assumed to be periodically continued onto the whole plane XOY. In Eqs. (8) and (9), ε is formally defined as a small parameter because expansions in ε around the point $\varepsilon = 0$ are used. $T(x, y)$ and $B(x, y)$ are assumed to be infinitely differentiable periodic functions. Without any loss of generality, it is assumed that

$$\int_{-L}^{L}\int_{-L}^{L} T(x, y)\,\mathrm{d}x\,\mathrm{d}y = \int_{-L}^{L}\int_{-L}^{L} B(x, y)\,\mathrm{d}x\,\mathrm{d}y = 0\,, \tag{11}$$

i.e., the mean amplitudes of T and B with respect to the planes $z = \pm b$ are equal to zero. The channel has a spatially periodic structure and is made of unit cells defined as:

$$Q := \big\{(x, y, z) \in \mathbb{R}^3 :\ -L \leqslant x \leqslant L,\ -L \leqslant y \leqslant L,\ S^{-}(x, y) < z < S^{+}(x, y)\big\}\,.$$

Let $\mathbf{u} = \mathbf{u}(x, y, z)$ be the velocity vector, and $p = p(x, y, z)$ the pressure. The fluid is governed by the Navier–Stokes equations

$$\begin{aligned} \mu\nabla^2\mathbf{u} &= \nabla p + \rho\mathbf{u}\cdot\nabla\mathbf{u}, \\ \nabla\cdot\mathbf{u} &= 0 \end{aligned} \tag{12}$$

with the boundary conditions

$$\mathbf{u} = \mathbf{0} \quad \text{on} \quad S^{\pm}. \tag{13}$$

The solution $\mathbf{u}$ of (12)–(13) belongs to the class of periodic functions with period $2L$ in x and y. An overall external gradient pressure is applied along the x-direction. It can be described by a constant jump $2L|\overline{\nabla p}|$ along the x-axis of the periodic cell

$$p(x+2L,y,z)-p(x,y,z)=-2L|\overline{\nabla p}|. \tag{14}$$

Let $\mathbf{u}=(u,v,w)$ be a solution of the problem (12)–(14), and let $\overline{u}$ be the average x-component of the velocity over the unit cell Q

$$\overline{u}=\frac{1}{|Q|}\int_0^L\int_0^L \mathrm{d}x\,\mathrm{d}y\int_{S^-(x,y)}^{S^+(x,y)} u(x,y,z)\,\mathrm{d}z\,, \tag{15}$$

where $|Q|$ is the volume of the channel. (11) implies

$$|Q|=\int_{-L}^{L}\int_{-L}^{L}\mathrm{d}x\,\mathrm{d}y\int_{S^-(x,y)}^{S^+(x,y)}\mathrm{d}z\;=8bL^2. \tag{16}$$

For convenience, dimensionless quantities indicated by primes are introduced:

$$(x,y,z)=l(x',y',z'),\quad \mathbf{u}=\frac{l^2|\overline{\nabla p}|}{\mu}\,\mathbf{u}',\quad p=l|\overline{\nabla p}|\;p'. \tag{17}$$

Equations (12)–(14) take the following dimensionless form:

$$\begin{aligned}\nabla'^2\mathbf{u}'&=\nabla' p'+\mathcal{R}(\mathbf{u}'\cdot\nabla)\mathbf{u}',\\ \nabla'\cdot\mathbf{u}'&=0,\end{aligned} \tag{18}$$

$$\mathbf{u}'=\mathbf{0}\quad\text{on}\quad S^{\pm} \tag{19}$$

and

$$p'(x'+\pi,y',z')-p'(x'-\pi,y',z')=-2\pi, \tag{20}$$

where the Reynolds number is introduced by (5). Then, the velocity $\mathbf{u}'$ for Poiseuille flow ($\varepsilon=0$) becomes

$$\mathbf{u}'_0(x',y',z')=\frac{1}{2}\left(b'^2-z'^2,\;0,\;0\right), \tag{21}$$

where $b=lb'$. Dimensionless equations of the walls (8)–(9) become

$$z'=S'^{+}(x',y')\equiv b'\left[1+\varepsilon T'(x',y')\right], \tag{22}$$

$$z'=S'^{-}(x',y')\equiv -b'\left[1+\varepsilon B'(x',y')\right], \tag{23}$$

where for instance $T'(x',y')=T(\ell x',\ell y')$. The volume of the dimensionless unit cell $|\tau|$ is equal to $8\pi^2 b$.

Since the dimensionless velocity $\mathbf{u}'$ depends on $\mathcal{R}$, its average first component can be considered as a function of the variable $\mathcal{R}$

$$\overline{u'}=\frac{1}{|\tau|}\int_{-\pi}^{\pi}\int_{-\pi}^{\pi}\mathrm{d}x'\mathrm{d}y'\int_{S'^-(x',y')}^{S'^+(x',y')}u'(x',y',z')\mathrm{d}z'=f(\mathcal{R}). \tag{24}$$

It is convenient to rewrite the dimensional equation (10) by defining a local Reynolds number, a dimensionless velocity $\overline{u^*}$ and a dimensionless pressure p^* as

$$\mathcal{R}_{\mathrm{loc}}=\frac{\rho U_0\ell}{\mu}, \tag{25a}$$

$$\mathbf{u}=U_0\mathbf{u}^*,\quad p=\frac{U_0\mu}{\ell}p^*, \tag{25b}$$

where U_0 is the local characteristic velocity in the channel. It is easily seen that

$$\frac{\mathcal{R}_{\rm loc}}{\mathcal{R}}\overline{u^*} = \overline{u'} \quad \text{and} \quad \frac{\mathcal{R}_{\rm loc}}{\mathcal{R}}|\overline{\nabla p^*}| = 1. \tag{26}$$

Concerning the second of Eqs. (26), it is worth noting that the dimensionless external gradient $\overline{\nabla p'}$ is equal to -1 as a consequence of (20). Substitution of (26) into (24) yields

$$\overline{u^*} = |\overline{\nabla p^*}|\ f(\mathcal{R}_{\rm loc}|\overline{\nabla p^*}|). \tag{27}$$

In order to invert the function (27), it is convenient to introduce the dimensionless variable $X = \mathcal{R}_{\rm loc}|\overline{\nabla p^*}|$. Then, (27) becomes

$$\mathcal{R}_{\rm loc}\overline{u^*} = Xf(X). \tag{28}$$

Let $X = H(Y)$ be the inverse function to $Y = Xf(X)$. Then, $X = H(\mathcal{R}_{\rm loc}\overline{u^*})$ which can be written in the form of a nonlinear dimensionless Darcy's law

$$|\overline{\nabla p^*}| = \frac{1}{\mathcal{R}_{\rm loc}} H(\mathcal{R}_{\rm loc}\overline{u^*}). \tag{29}$$

The function $X = H(Y)$ is analytic at zero and $H(0) = 0$ by the inverse function theorem, since it is inverse to $Y(X) = Xf(X)$ and the derivative $Y'(0) = f(0)$ is equal to the averaged velocity (24) which is not vanish. Therefore, (29) can locally be written in the form

$$|\overline{\nabla p^*}| = \sum_{k=1}^{\infty} h_k \overline{u^*}^k. \tag{30}$$

The first term h_1 yields the linear Darcy's law (1). The coefficients h_k ($k > 1$) determine the nonlinear corrections. In order to calculate h_k, it is necessary to find $\overline{u}'$ from the problem (18)–(20) with the parameter $\mathcal{R}$, i.e., to construct the function $f(\mathcal{R})$ by (24). Further, the function $X = H(Y)$ is constructed as the inverse to $Y = Xf(X)$. Ultimately, $H(Y)$ is expanded as a Taylor series near zero to determine h_k in (30).

Additional comments can be made on the definition of $\mathcal{R}_{\rm loc}$. Usually, a local Reynolds number is defined as $\mathcal{R}e_{\rm loc} = \frac{\rho U_0 2b}{\mu}$. The ratio $\frac{\mathcal{R}e_{\rm loc}}{\mathcal{R}_{\rm loc}}$ equal to $2b'$ is of order 1 and in most computations $b' = 1$. Therefore, $\mathcal{R}e_{\rm loc}$ and $\mathcal{R}_{\rm loc}$ are of the same order.

Finally, channels with side walls are particular $3D$ cases of (22)–(23). They can be derived from plane channels by perturbations along the y-axis in such a way that walls are touching along lines parallel to it. Analogous configurations were calculated in [16] without any numerical difficulty.

3 Small Reynolds numbers

3.1 General method for small Reynolds numbers

In order to solve the problem (18)–(20) and to investigate the properties of the solution, the unknown functions are expanded in $\mathcal{R}$ and ε; then, the method of separated variables is applied. For brevity, primes are suppressed in the dimensionless values up to Sect. 5.2.

For our purposes, it is convenient to expand $T(x, y)$ and $B(x, y)$ in Fourier series which because of (40) can be simplified as

$$T(x, y) = \sum_{s,t=0}^{\infty} T_{s,t} \cos sx \cos ty, \quad B(x, y) = \sum_{s,t=0}^{\infty} B_{s,t} \cos sx \cos ty, \tag{31}$$

where $T_{0,0} = B_{0,0} = 0$ in accordance with (11).

Look for a solution in the form of a series of $\mathcal{R}$

$$\mathbf{u}(x, y, z) = \sum_{k=0}^{\infty} \mathbf{u}^{(k)}(x, y, z)\mathcal{R}^k, \quad p(x, y, z) = \sum_{k=0}^{\infty} p^{(k)}(x, y, z)\mathcal{R}^k. \tag{32}$$

This latter representation holds for sufficiently small Reynolds numbers. Substitute (32) into (18) and select the coefficients with the same powers of $\mathcal{R}$. For $\mathcal{R}^0$,

$$\begin{aligned} \nabla^2 \mathbf{u}^{(0)} &= \nabla p^{(0)}, \\ \nabla \cdot \mathbf{u}^{(0)} &= 0. \end{aligned} \tag{33}$$

For $\mathcal{R}^k$

$$\begin{aligned} \nabla^2 \mathbf{u}^{(k)} &= \nabla p^{(k)} + \sum_{n=0}^{k-1} (\mathbf{u}^{(k-n-1)} \cdot \nabla) \mathbf{u}^{(n)}, \\ \nabla \cdot \mathbf{u}^{(k)} &= 0, \quad k = 1, 2, 3, \ldots \end{aligned} \tag{34}$$

(33)–(34) is a cascade of equations in the channel $S^-(x, y) < z < S^+(x, y)$. The no-slip boundary condition (18) and the jump of $p^{(0)}$ along the x-axis are imposed.

Each problem of the cascade can be solved by an expansion in ε:

$$\mathbf{u}^{(k)} = \sum_{m=0}^{\infty} \mathbf{u}_m^{(k)} \varepsilon^m, \quad p^{(k)} = \sum_{m=0}^{\infty} p_m^{(k)} \varepsilon^m, \quad k = 0, 1, 2, \ldots \tag{35}$$

The zeroth terms are known from the Poiseuille flow:

$$\mathbf{u}_0^{(0)} = \left(\frac{b^2 - z^2}{2}, 0, 0 \right), \quad p_0^{(0)} = x. \tag{36}$$

In each problem, (34) $\mathbf{u}^{(k)}$ and $p^{(k)}$ are unknown while $\mathbf{u}^{(k-1)}, p^{(k-1)}, \ldots, \mathbf{u}^{(1)}, p^{(1)}$ are calculated in the previous steps of the cascade. Hence, at each step of the cascade, we have the following linear problem for the straight channel $-b < z < b$:

$$\begin{aligned} \nabla^2 \mathbf{u}_m^{(k)} &= \nabla p_m^{(k)} + \mathbf{F}_m^{(k)}, \\ \nabla \cdot \mathbf{u}_m^{(k)} &= 0, \quad m = 0, 1, 2, \ldots \end{aligned} \tag{37}$$

with the boundary conditions [16]

$$\begin{aligned} \mathbf{u}_m^{(k)}(x, y, b) &= -\sum_{n=1}^{m} \frac{(bT)^n}{n!} \frac{\partial^n \mathbf{u}_{m-n}^{(k)}}{\partial z^n}(x, y, b), \\ \mathbf{u}_m^{(k)}(x, y, -b) &= -\sum_{n=1}^{m} \frac{(-bB)^n}{n!} \frac{\partial^n \mathbf{u}_{m-n}^{(k)}}{\partial z^n}(x, y, -b). \end{aligned} \tag{38}$$

Here,

$$\mathbf{F}^{(0)} = \mathbf{0}, \quad \mathbf{F}^{(k)} = \sum_{n=0}^{k-1} (\mathbf{u}^{(k-n-1)} \cdot \nabla) \mathbf{u}^{(k)} = \sum_{n=0}^{\infty} \mathbf{F}_m^{(k)} \varepsilon^m, \quad k = 1, 2, \ldots \tag{39}$$

3.2 Symmetric channels

Consider the special case of the channels satisfying the symmetry conditions

$$T(x, y) = T(-x, y) = T(x, -y), \quad B(x, y) = B(-x, y) = B(x, -y). \tag{40}$$

Then, the expansion (30) for small $\mathcal{R}$ is simplified as

$$|\overline{\nabla p^*}| = h_1 \overline{u^*} + \sum_{k=1}^{\infty} \beta_k \overline{u^*}^{2k+1}. \tag{41}$$

The first two terms $h_1\overline{u^*} + \beta_1\overline{u^*}^3$ yield the cubic filtration law (6). The expansion (41) follows from the following mathematical result proved in the Appendix.

Let $\mathbf{u}' = (u', v', w')$ and p' be a solution of the problem (18)–(20) for sufficiently small $\mathcal{R}$. Then, the average x- component $\overline{u'}$ of the velocity can be expressed by (24), where $f(\mathcal{R})$ is an even function analytic at $\mathcal{R} = 0$.

Formula (41) follows from this assertion, since the function $f(X)$ is even and since the odd function $Xf(X)$ yields the odd inverse function $H(Y)$. (41) is just the Taylor series of an odd function at zero.

3.3 Examples for various channels

In the present section, examples for symmetric and non-symmetric channels are explicitly calculated with the accuracy $O(\mathcal{R}^2)$ in the Reynolds number and the accuracy $O(\varepsilon^8)$ or $O(\varepsilon^6)$ in ε. These examples confirm the first terms of the series (41) and lead to the conjecture that the cubic filtration law (6) holds also for non-symmetric channels. It is worth noting that it is impossible to find a channel corresponding to the example of the rotational flow from [13] for which the average velocity satisfies the quadratic equation (4).

Consider the two-dimensional channel bounded by walls of the form (compare to (8)–(9))

$$z = \pm(1 + \varepsilon\cos x), \tag{42}$$

i.e., $T(x) = B(x) = \cos x$. Application of the algorithm described in Sect. 3 up to $O(\varepsilon^9)$ yields

$$\begin{aligned}\overline{u'} = \frac{1}{3} &- 1.197869\varepsilon^2 + 2.1879319\varepsilon^4 - 3.5207469\varepsilon^6 + 6.00297165\varepsilon^8 \\ &+ \mathcal{R}^2(-0.0001423718\varepsilon^2 + 0.0018613318\varepsilon^4 - 0.0123671532\varepsilon^6 + 0.0569631460\varepsilon^8).\end{aligned} \tag{43}$$

This is the function (24) calculated up to $O(\varepsilon^9)$. In order to determine the dependence (30) up to $O(\mathcal{R}^3)$ in accordance with Sect. 2, invert the function

$$Y = X(f_0 + f_1X^2), \tag{44}$$

where $f(X) = f_0 + f_1X^2 + O(X^3)$. The inverse function can be found as:

$$H(Y) = X = Y(h_1 + h_2Y + h_3Y^2) + O(Y^4). \tag{45}$$

Substitution of (45) into (44) yields

$$Y = Y(h_1 + h_2Y + h_3Y^2)(f_0 + f_1Y^2h_1^2) + O(Y^4). \tag{46}$$

Take the coefficients in the same powers of Y and determine the coefficients of the function $H(Y)$. Simple calculations yield

$$H(Y) = Y\left(\frac{1}{f_0} - \frac{f_1}{f_0^4}Y^2\right) + O(Y^4). \tag{47}$$

Introduction of (47) into (43) and use of (29) yield

$$|\overline{\nabla p^*}| = \frac{3 + 2.69839\varepsilon^2 - 3.88887\varepsilon^4}{1 - 2.69414\varepsilon^2 + 2.03519\varepsilon^4}\,\overline{u^*} + \frac{0.0115321\varepsilon^2 + 0.0390439\varepsilon^4}{1 + 2.08497\varepsilon^2 - 4.53451\varepsilon^4}\,\mathcal{R}_{\mathrm{loc}}^2\overline{u^*}^3. \tag{48}$$

Here, the coefficients are written by the application of Padé approximation in ε.

Consider the two-dimensional non-symmetric channel bounded by walls of the form

$$z = 1 + \varepsilon\cos x, \quad z = -1 - \varepsilon\cos\left(\frac{3}{2} - 2x\right). \tag{49}$$

Application of the algorithm described in Sect. 3 up to $O(\varepsilon^7)$ implies

$$\begin{aligned}\overline{u'} = \frac{1}{3} &- 1.1532\varepsilon^2 + 0.0120753\varepsilon^3 + 3.09254\varepsilon^4 - 0.042636\varepsilon^5 - 10.3416\varepsilon^6 \\ &+ \mathcal{R}^2(-0.000626762\varepsilon^2 + 0.0000108797\varepsilon^3 + 0.00993578\varepsilon^4 - 0.000249599\varepsilon^5 - 0.0938563\varepsilon^6).\end{aligned} \tag{50}$$

Table 1 Walls and velocity $\overline{u'}$ (24) for various channels

$T(x)=\cos(x)$, $B(x)=\cos(2x)$,
$\frac{1}{3}-1.15320\varepsilon^2+0.17071\varepsilon^3+3.09254\varepsilon^4+\mathcal{R}^2(-0.00063\varepsilon^2+0.00015\varepsilon^3+0.00994\varepsilon^4)$
$T(x)=\cos(x)$, $B(x)=\cos\left(2x-\frac{1}{5}\right)$,
$\frac{1}{3}-1.15320\varepsilon^2+0.16730\varepsilon^3+3.09254\varepsilon^4+\mathcal{R}^2(-0.00063\varepsilon^2+0.00015\varepsilon^3+0.00994\varepsilon^4)$
$T(x)=\cos(x)$, $B(x)=\cos\left(2x-\frac{2}{5}\right)$,
$\frac{1}{3}-1.15320\varepsilon^2+0.15723\varepsilon^3+3.09254\varepsilon^4+\mathcal{R}^2(-0.00063\varepsilon^2+0.00014\varepsilon^3+0.00994\varepsilon^4)$
$T(x)=\cos(x)$, $B(x)=\cos\left(2x-\frac{1}{2}\right)$,
$\frac{1}{3}-1.15320\varepsilon^2+0.14981\varepsilon^3+3.09254\varepsilon^4+\mathcal{R}^2(-0.00063\varepsilon^2+0.00013\varepsilon^3+0.00994\varepsilon^4)$
$T(x)=\cos(x)$, $B(x)=\cos(2x-1)$,
$\frac{1}{3}-1.15320\varepsilon^2+0.09223\varepsilon^3+3.09254\varepsilon^4+\mathcal{R}^2(-0.00063\varepsilon^2+0.00008\varepsilon^3+0.00994\varepsilon^4)$
$T(x)=\cos(x)$, $B(x)=\cos\left(2x-\frac{3}{2}\right)$,
$\frac{1}{3}-1.15320\varepsilon^2+0.01208\varepsilon^3+3.09254\varepsilon^4+\mathcal{R}^2(-0.00063\varepsilon^2+0.00001\varepsilon^3+0.00994\varepsilon^4)$
$T(x)=\cos(x)$, $B(x)=\cos(2x-2)$,
$\frac{1}{3}-1.15320\varepsilon^2-0.07104\varepsilon^3+3.09254\varepsilon^4+\mathcal{R}^2(-0.00063\varepsilon^2-0.00006\varepsilon^3+0.00994\varepsilon^4)$
$T(x)=\cos(x)$, $B(x)=\cos\left(2x-\frac{5}{2}\right)$,
$\frac{1}{3}-1.15320\varepsilon^2-0.13676\varepsilon^3+3.09254\varepsilon^4+\mathcal{R}^2(-0.00063\varepsilon^2-0.00012\varepsilon^3+0.00994\varepsilon^4)$
$T(x)=\cos(x)$, $B(x)=\cos(2x-3)$,
$\frac{1}{3}-1.15320\varepsilon^2-0.16900\varepsilon^3+3.09254\varepsilon^4+\mathcal{R}^2(-0.00063\varepsilon^2-0.00015\varepsilon^3+0.00994\varepsilon^4)$
$T(x)=\cos(x)$, $B(x)=\cos\left(2x-\frac{31}{10}\right)$,
$\frac{1}{3}-1.15320\varepsilon^2-0.17056\varepsilon^3+3.09254\varepsilon^4+\mathcal{R}^2(-0.00063\varepsilon^2-0.00015\varepsilon^3+0.00994\varepsilon^4)$
$T(x)=\cos(x)$, $B(x)=\cos(3x)$,
$\frac{1}{3}-1.63718\varepsilon^2+9.33468\varepsilon^4+\mathcal{R}^2(-0.00072\varepsilon^2+0.01817\varepsilon^4)$
$T(x)=\cos(x)$, $B(x)=\cos\left(3x+\frac{1}{2}\right)$,
$\frac{1}{3}-1.63718\varepsilon^2+9.34093\varepsilon^4+\mathcal{R}^2(-0.00072\varepsilon^2+0.01818\varepsilon^4)$
$T(x)=\cos(x)$, $B(x)=\cos(3x+1)$,
$\frac{1}{3}-1.63718\varepsilon^2+9.35815\varepsilon^4+\mathcal{R}^2(-0.00072\varepsilon^2+0.01819\varepsilon^4)$
$T(x)=\cos(x)$, $B(x)=\cos\left(3x+\frac{3}{2}\right)$,
$\frac{1}{3}-1.63718\varepsilon^2+9.38214\varepsilon^4+\mathcal{R}^2(-0.00072\varepsilon^2+0.01821\varepsilon^4)$
$T(x)=\cos(x)$, $B(x)=\cos(3x+2)$,
$\frac{1}{3}-1.63718\varepsilon^2+9.40700\varepsilon^4+\mathcal{R}^2(-0.00072\varepsilon^2+0.01824\varepsilon^4)$
$T(x)=\cos(x)$, $B(x)=\cos\left(3x+\frac{5}{2}\right)$,
$\frac{1}{3}-1.63718\varepsilon^2+9.42667\varepsilon^4+\mathcal{R}^2(-0.00072\varepsilon^2+0.01825\varepsilon^4)$

The dependence (30) takes the form

$$|\overline{\nabla p^*}| = \frac{3+277.693\varepsilon+10.9529\varepsilon^2+744.693\varepsilon^3}{1+92.5643\varepsilon+0.191342\varepsilon^2-71.9692\varepsilon^3}\,\overline{u^*} + \frac{0.0507677\varepsilon^2+7.94934\varepsilon^3}{1+156.6\varepsilon+4.73248\varepsilon^2+315.481\varepsilon^3}\,\mathcal{R}_{\rm loc}^2\overline{u^*}^3. \tag{51}$$

For other channels, calculations are performed up to $O(\varepsilon^5)$. The results are presented in Table 1. In all the formulae, the term with $\mathcal{R}$ vanishes. It follows from the relation between (44) and (47) that Darcy's laws for all channels do not contain a quadratic term.

It is worth noting that all the numbers are given with a very high precision. The continuity equation $\nabla\cdot\mathbf{u}=0$ is verified up to 10^{-12}, the differential equations (118) are solved with the precision 10^{-14}, the boundary condition (13) holds up to 10^{-8}. The numerical coefficients in the table are valid at least up to 10^{-6}.

4 Algorithm for arbitrary Reynolds numbers

A general algorithm for arbitrary Reynolds numbers was developed in [15] for Couette flow. The same algorithm can be applied to Poiseuille flow by replacing the zero Couette velocity $\mathbf{u}_0(x,y,z)=(z,0,0)$ by $\mathbf{u}_0(x,y,z)=\frac{1}{2}\left(b^2-z^2,\,0,\,0\right)$. The main difficulty is due to the fact that the Airy functions used in [15] must be replaced by some numerically calculated functions which cannot be expressed in terms of known standard functions.

In the next three subsections, the general algorithm is described and detailed up to $O(\varepsilon^3)$. Section 5.2 contains a numerical example.

4.1 General

In the present subsection, there is no assumption on the symmetry of the functions $T(x, y)$ and $B(x, y)$ like (31). Generally, it is convenient to represent these periodic functions by their complex Fourier series

$$T(x, y) = \sum_{s,t=-\infty}^{\infty} T_{st} e^{i(sx+ty)}, \quad B(x, y) = \sum_{s,t=-\infty}^{\infty} B_{st} e^{i(sx+ty)}, \tag{52}$$

where i stands for the imaginary unity; s and t run over integer numbers from $-\infty$ to $+\infty$. Since the functions $T(x, y)$ and $B(x, y)$ are real, their complex Fourier coefficients satisfy the relations

$$T_{-s,-t} = T_{st}^*, \quad B_{-s,-t} = B_{st}^*, \tag{53}$$

where $*$ stands for complex conjugation. It follows from (11) that $T_{00} = B_{00} = 0$. Moreover, it is now assumed that the Reynolds number $\mathcal{R}$ can be arbitrary at least theoretically.

Expansions in ε are used for the velocity and for the pressure

$$\mathbf{u} = \sum_{k=0}^{\infty} \mathbf{u}_k \varepsilon^k, \quad p = \sum_{k=0}^{\infty} p_k \varepsilon^k. \tag{54}$$

Each coefficient in (54) is looked for in the form of a double Fourier series

$$\mathbf{u}_k(x, y, z) = \sum_{s,t=-\infty}^{\infty} \mathbf{u}_{kst}(z) e^{i(sx+ty)}, \quad p_k = \sum_{s,t=-\infty}^{\infty} p_{kst}(z) e^{i(sx+ty)}. \tag{55}$$

Substitution of (54)–(55) into (18) and comparison of the coefficients in ε^k yield the cascade of equations

$$\begin{aligned} &\nabla^2 \mathbf{u}_k = \nabla p_k + \mathcal{R}(\mathbf{u}_k \cdot \nabla \mathbf{u}_0 + \mathbf{u}_0 \cdot \nabla \mathbf{u}_k) + \mathcal{R} \sum_{m=1}^{k-1} \mathbf{u}_m \cdot \nabla \mathbf{u}_{k-m}, \\ &\nabla \cdot \mathbf{u}_k = 0. \end{aligned} \tag{56}$$

The boundary conditions expanded in ε have the same form (38) as for small $\mathcal{R}$.

4.2 First-order approximation

The study in the present section is performed with the accuracy $O(\varepsilon^2)$. Hence, all formulae are written explicitly up to $O(\varepsilon^3)$. The zeroth term in ε is given by (21). The first-order approximation problem is obtained from (56) with $k = 1$

$$\begin{aligned} &\nabla^2 u_1 = \frac{\partial p_1}{\partial x} + \mathcal{R}\left[\frac{1}{2}(b^2 - z^2)\frac{\partial u_1}{\partial x} - z w_1\right], \\ &\nabla^2 v_1 = \frac{\partial p_1}{\partial y} + \frac{\mathcal{R}(b^2 - z^2)}{2}\frac{\partial v_1}{\partial x}, \\ &\nabla^2 w_1 = \frac{\partial p_1}{\partial z} + \frac{\mathcal{R}(b^2 - z^2)}{2}\frac{\partial w_1}{\partial x}, \\ &\frac{\partial u_1}{\partial x} + \frac{\partial v_1}{\partial y} + \frac{\partial w_1}{\partial z} = 0, \end{aligned} \tag{57}$$

where $\mathbf{u}_1 = (u_1, v_1, w_1)$. The boundary conditions take the form

$$u_1(x, y, b) = b^2 T(x, y), \ u_1(x, y, -b) = b^2 B(x, y), \ v_1(x, y, \pm b) = w_1(x, y, \pm b) = 0. \tag{58}$$

Substitute the Fourier series (52) and (55) with $k = 1$ into (57)–(58) and take the coefficients of $e^{i(sx+ty)}$. Equations (57) are separated into four ordinary differential equations

$$\frac{\mathrm{d}^2 u_{1st}}{\mathrm{d}z^2} - \omega_{st}^2 u_{1st} = isp_{1st} + is\mathcal{R}\frac{b^2 - z^2}{2}u_{1st} - \mathcal{R}zw_{1st}, \tag{59a}$$

$$\frac{\mathrm{d}^2 v_{1st}}{\mathrm{d}z^2} - \omega_{st}^2 v_{1st} = itp_{1_y} + is\mathcal{R}\frac{1}{2}(b^2 - z^2)\frac{\mathrm{d}v_{1st}}{\mathrm{d}x}, \tag{59b}$$

$$\frac{\mathrm{d}^2 w_{1st}}{\mathrm{d}z^2} - \omega_{st}^2 w_{1st} = \frac{\mathrm{d}p_{1st}}{\mathrm{d}z} + is\mathcal{R}\frac{1}{2}(b^2 - z^2)\frac{\mathrm{d}w_{1st}}{\mathrm{d}x}, \tag{59c}$$

$$isu_{1st} + itv_{1st} + \frac{\mathrm{d}w_{1st}}{\mathrm{d}z} = 0, \tag{59d}$$

where $\omega_{st}^2 = s^2 + t^2$. The boundary conditions (58) become

$$u_{1st}(b) = b^2 T_{st},\ u_{1st}(-b) = b^2 B_{st},\ v_{1st}(\pm b) = w_{1st}(\pm b) = 0. \tag{60}$$

The term $s = t = 0$ could be written separately since it has another form. It is easily seen that the condition $T_{00} = B_{00} = 0$ implies the zero boundary conditions for $u_{100}(z)$. Direct calculations yield $u_{100}(z) \equiv v_{100}(z) \equiv w_{100}(z) \equiv 0$.

Equation (59a) is differentiated and multiplied by is, equation (59b) is differentiated and multiplied by it, (59c) is multiplied by ω_{st}^2 and the results are added. Then, equation (59d) yields a differential equation closely related to the celebrated Orr–Sommerfeld equation discussed in the stability theory [22]

$$\frac{\mathrm{d}^4 w_{1st}}{\mathrm{d}z^4} - 2\omega_{st}^2\frac{\mathrm{d}^2 w_{1st}}{\mathrm{d}z^2} + \omega_{st}^4 w_{1st} = is\mathcal{R}\left[\frac{1}{2}(b^2 - z^2)\frac{\mathrm{d}^2 w_{1st}}{\mathrm{d}z^2} + \left(1 - \omega_{st}^2\frac{b^2 - z^2}{2}\right)w_{1st}\right] \tag{61}$$

with the boundary conditions

$$w_{1st}(\pm b) = 0,\ \frac{\mathrm{d}w_{1st}}{\mathrm{d}z}(b) = -isb^2 T_{st},\ \frac{\mathrm{d}w_{1st}}{\mathrm{d}z}(-b) = -isb^2 B_{st}. \tag{62}$$

Unfortunately, the ordinary differential equation (61) cannot be solved in terms of the known elementary and special functions (compare to [22]); it is solved numerically by the following method. First, Eq. (61) is reduced to a system of ordinary first-order equations

$$\begin{aligned} &\frac{\mathrm{d}w_{1st}}{\mathrm{d}z} = w_1,\ \frac{\mathrm{d}w_1}{\mathrm{d}z} = w_2,\ \frac{\mathrm{d}w_2}{\mathrm{d}z} = w_3, \\ &\frac{\mathrm{d}w_3}{\mathrm{d}z} = 2\omega_{st}^2 w_2 - \omega_{st}^4 w_{1st} + is\mathcal{R}\left[\frac{1}{2}(b^2 - z^2)w_2 + \left(1 - \omega_{st}^2\frac{b^2 - z^2}{2}\right)w_{1st}\right]. \end{aligned} \tag{63}$$

The boundary conditions (62) are written for the system (63)

$$w_{1st}(\pm b) = 0,\ w_1(b) = -isb^2 T_{st},\ w_1(-b) = -isb^2 B_{st}. \tag{64}$$

The problem (63)–(64) is transformed into a system of four differential equations of first order with the corresponding boundary conditions at the points $z = \pm b$:

$$w_{1st}(0) = 0, \quad w_1(0) = -\frac{isb^2}{2}(T_{st} + B_{st}), \quad w_2(0) = w_3(0) = 0. \tag{65}$$

The latter system is solved numerically by *Mathematica*© by use of the modified "shooting method" with an adaptive step of integration constructed on the basis of the Runge–Kutta method of fourth order. All computations are performed with the accuracy 10^{-16}. Convergence of the method is controlled by comparison of the derivatives of all orders from 1 to 4 in the integration points by two methods; first, by direct check of the system, and secondly, by interpolation in the neighbour integration points. Iterations are continued until the maximal difference between subsequent iterations becomes smaller than 0.01. The criterion of the absolute and respective precisions gives convergence for $\mathcal{R} = 10^7$ and $\mathcal{R} = 10^8$, respectively. The difference of the

results obtained by both methods does not exceed 0.1 % for $0 \le \mathcal{R} \le 10^7$. It is assumed that the method diverges if the accuracy is not reached by division of the interval $-b < z < b$ into 256,000 subintervals.

In order to determine $u_{1st}(z)$, multiply Eq. (59a) by t, Eq. (59b) by $-s$ and add the results

$$\frac{\mathrm{d}^2 U_{st}}{\mathrm{d}z^2} - \left(\omega_{st}^2 + is\mathcal{R}\frac{b^2 - z^2}{2}\right) U_{st} = -t\mathcal{R}z\, w_{1st}, \tag{66}$$

where $U_{st} = tu_{1st} - sv_{1st}$. The boundary conditions for U_{st} are derived from (60)

$$U_{st}(b) = tb^2 T_{st}, \quad U_{st}(-b) = tb^2 B_{st}. \tag{67}$$

The problem (66)–(67) is solved numerically with the numerically given right hand part of (66). The velocity components are found from the system

$$isu_{1st} + itv_{1st} = -\frac{\mathrm{d}w_{1st}}{\mathrm{d}z}, \quad tu_{1st} - sv_{1st} = U_{st}. \tag{68}$$

In particular,

$$u_{1st}(z) = \omega_{st}^{-2}\left[is\frac{\mathrm{d}w_{1st}}{\mathrm{d}z} + tU_{st}(z)\right]. \tag{69}$$

This is the final formula for the first approximation $u_{1st}(z)$, where w_{1st} and $U_{st}(z)$ are numerically found from the boundary value problems (61)–(62) and (66)–(67), respectively, for ordinary differential equations.

4.3 Second-order approximation

Consider now the second-order equations

$$\begin{aligned}
&\nabla^2 u_2 = \frac{\partial p_2}{\partial x} + \mathcal{R}\left[\frac{b^2 - z^2}{2}\frac{\partial u_2}{\partial x} - zw_2\right] + \mathcal{R}\left(u_1\frac{\partial u_1}{\partial x} + v_1\frac{\partial u_1}{\partial y} + w_1\frac{\partial u_1}{\partial z}\right),\\
&\nabla^2 v_2 = \frac{\partial p_2}{\partial y} + \mathcal{R}\frac{b^2 - z^2}{2}\frac{\partial v_2}{\partial x} + \mathcal{R}\left(u_1\frac{\partial v_1}{\partial x} + v_1\frac{\partial v_1}{\partial y} + w_1\frac{\partial v_1}{\partial z}\right),\\
&\nabla^2 w_2 = \frac{\partial p_2}{\partial z} + \mathcal{R}\frac{b^2 - z^2}{2}\frac{\partial w_2}{\partial x} + \mathcal{R}\left(\frac{u_1\partial w_1}{\partial x} + v_1\frac{\partial w_1}{\partial y} + w_1\frac{\partial w_1}{\partial z}\right),\\
&\frac{\partial u_2}{\partial x} + \frac{\partial v_2}{\partial y} + \frac{\partial w_2}{\partial z} = 0.
\end{aligned} \tag{70}$$

The boundary conditions have the form

$$\begin{aligned}
&u_2(x,y,b) = \frac{b^2}{2}T^2(x,y) - bT(x,y)\frac{\partial u_1}{\partial z}(x,y,b),\ u_2(x,y,-b) = \frac{b^2}{2}B^2(x,y) + bB(x,y),\\
&v_2(x,y,b) = -bT(x,y)\frac{\partial v_1}{\partial z}(x,y,b),\ v_2(x,y,-b) = bB(x,y)\frac{\partial v_1}{\partial z}(x,y,-b),\\
&w_2(x,y,b) = -bT(x,y)\frac{\partial w_1}{\partial z}(x,y,b),\ w_2(x,y,-b) = bB(x,y)\frac{\partial w_1}{\partial z}(x,y,-b).
\end{aligned} \tag{71}$$

It will be seen in the next subsection that only the term $u_{200}(z)$ from the representation (55) is needed for the calculation of the average velocity up to $O(\varepsilon^3)$. It is equivalent to look for solutions of Eq. (70) depending only on z:

$$\frac{\mathrm{d}^2 u_{200}}{\mathrm{d}z^2} = -\mathcal{R}z\, w_{200} + \mathcal{R}F(z),\ \frac{\mathrm{d}^2 v_{200}}{\mathrm{d}z^2} = \mathcal{R}F_v(z),\ \frac{\mathrm{d}^2 w_{200}}{\mathrm{d}z^2} = \frac{\mathrm{d}p_{200}}{\mathrm{d}z} + \mathcal{R}F_w(z),\ \frac{\mathrm{d}w_{200}}{\mathrm{d}z} = 0, \tag{72}$$

where the functions $F(z)$, $F_v(z)$ and $F_w(z)$ are $(0,0)$-Fourier coefficients of the functions included in the parentheses of the right hand part of (70). Further, only the explicit form of the function $F(z)$ is needed:

$$F(z) = \sum_{s,t} \left[w_{1st} \frac{\mathrm{d}u_{1,-s,-t}}{\mathrm{d}z} - i(su_{1st} + tv_{1st})u_{1,-s,-t} \right]. \tag{73}$$

Here, s and t run over integer numbers. One of the sums of (73) vanishes:

$$\sum_{s,t} su_{1st}u_{1,-s,-t} = \sum_{t} \sum_{s=1}^{\infty} [su_{1st}u_{1,-s,-t} + (-s)u_{1,-s,-t}u_{1st}] = 0. \tag{74}$$

Therefore, (73) can be simplified as:

$$F(z) = \sum_{s,t} \left[w_{1st} \frac{\mathrm{d}u_{1,-s,-t}}{\mathrm{d}z} - itv_{1st}u_{1,-s,-t} \right]. \tag{75}$$

Since in the two-dimensional case $v_{1st} = 0$, the second term in (75) vanishes.

Consider the $(0,0)$-Fourier coefficient of the boundary values $w_2(x, y, b)$ from (71). Application of the $(0,0)$-Fourier coefficient of (59d) yields

$$w_{200}(b) = ib \sum_{s,t} T_{st}(su_{1,-s,-t} + tv_{1,-s,-t}).$$

Use of the boundary conditions (60) yields zero in a way similar to (74)

$$w_{200}(b) = ib^3 \sum_{s,t} T_{st}sT_{-s,-t} = 0.$$

The same arguments applied to the boundary condition at $z = -b$ also yield $w_{200}(-b) = 0$. Therefore, the differential equation $\frac{\mathrm{d}w_{200}}{\mathrm{d}z} = 0$ with $w_{200}(\pm b) = 0$ has only the zero solution. Substitute $w_{200}(z) \equiv 0$ into the first equation (72) and find

$$u_{200}(z) = \mathcal{R} \int_{-b}^{z} (z - \tau)F(\tau)\mathrm{d}\tau + C_1 z + C_2, \tag{76}$$

where C_1 and C_2 are undetermined constants.

The boundary conditions for $u_{200}(z)$ are derived from the boundary conditions (71)

$$\begin{aligned} u_{200}(b) &= b \sum_{s,t} T_{st} \left[\frac{b}{2} T_{-s,-t} - \frac{\mathrm{d}u_{1,-s,-t}}{\mathrm{d}z}(b) \right], \\ u_{200}(-b) &= b \sum_{s,t} B_{st} \left[\frac{b}{2} B_{-s,-t} + \frac{\mathrm{d}u_{1,-s,-t}}{\mathrm{d}z}(-b) \right], \end{aligned} \tag{77}$$

where $\frac{\mathrm{d}u_{1,-s,-t}}{\mathrm{d}z}(\pm b)$ was found in Sect. 4.2. Substitution of (77) into (76) yields formulae for the constants

$$\begin{aligned} C_1 &= \frac{1}{2b} \left[u_{200}(b) - u_{200}(-b) - \mathcal{R} \int_{-b}^{z} (z - \tau)F(\tau)\mathrm{d}\tau \right], \\ C_2 &= \frac{1}{2} \left[u_{200}(b) + u_{200}(-b) - \mathcal{R} \int_{-b}^{z} (z - \tau)F(\tau)\mathrm{d}\tau \right]. \end{aligned} \tag{78}$$

4.4 Average velocity up to $O(\varepsilon^3)$

For shortness, introduce the notation "$\simeq$" for equalities valid up to $O(\varepsilon^3)$. The average velocity over the unit cell τ can be approximately calculated by

$$\overline{u} \simeq \overline{u_0} + \varepsilon\overline{u_1} + \varepsilon^2\overline{u_2}, \tag{79}$$

where

$$\overline{a} := \frac{1}{|Q|}\int_Q a(x, y, z)\mathrm{d}x\mathrm{d}y\mathrm{d}z \tag{80}$$

denotes the triple integral over the fluid domain Q. Following [16], calculate

$$\begin{aligned}\overline{a} &= \frac{1}{8\pi b^2}\int_{-\pi}^{\pi}\int_{-\pi}^{\pi}\mathrm{d}x\mathrm{d}y\int_{-b(1+\varepsilon B)}^{b(1+\varepsilon T)} a(x, y, z)\mathrm{d}z\\ &\simeq \frac{1}{8\pi b^2}\int_{-\pi}^{\pi}\int_{-\pi}^{\pi}\mathrm{d}x\mathrm{d}y\left\{\int_{-b}^{b} a(x, y, z)\mathrm{d}z + \varepsilon b[T(x, y)a(x, y, b) + B(x, y)a(x, y, -b)]\right.\\ &\quad\left. + \frac{\varepsilon^2 b^2}{2}\left[T^2(x, y)\frac{\partial a}{\partial z}(x, y, b) - B^2(x, y)\frac{\partial a}{\partial z}(x, y, -b)\right]\right\}.\end{aligned} \tag{81}$$

Application of (81) to $u_0 = \frac{1}{2}(b^2 - z^2)$ yields

$$\overline{u_0} \simeq b^2\left(\frac{1}{3} - \frac{\varepsilon^2 G_0}{4}\right), \tag{82}$$

where G_0 is the $(0, 0)$-Fourier coefficient of the function $T^2(x, y) + B^2(x, y)$, i.e.,

$$G_0 = \frac{1}{4\pi^2}\int_{-\pi}^{\pi}\int_{-\pi}^{\pi}[T^2(x, y) + B^2(x, y)]\mathrm{d}x\mathrm{d}y = \sum_{s,t}(|T_{st}|^2 + |B_{st}|^2). \tag{83}$$

Application of (81) to $\varepsilon\overline{u_1}$ yields

$$\varepsilon\overline{u_1} \simeq \frac{\varepsilon}{8\pi^2 b^2}\int_{-\pi}^{\pi}\int_{-\pi}^{\pi}\mathrm{d}x\mathrm{d}y\left\{\int_{-b}^{b} u_1(x, y, z)\mathrm{d}z + \varepsilon b[T(x, y)u_1(x, y, b) + B(x, y)u_1(x, y, -b)]\right\}. \tag{84}$$

The triple integral in (84) can be calculated by changing the order of integration

$$\int_{-b}^{b}\mathrm{d}z\int_{-\pi}^{\pi}\int_{-\pi}^{\pi} u_1(x, y, z)\mathrm{d}x\mathrm{d}y = 0. \tag{85}$$

Here, it is used that the $(0, 0)$-Fourier coefficients of the function $u_1(x, y, z)$ vanish. Substitution of the boundary conditions (58) into (84) yields

$$\varepsilon\overline{u_1} \simeq \frac{\varepsilon^2 b^2}{2}G_0. \tag{86}$$

The zeroth order of the third term $\overline{u_2}$ of (79) is calculated as

$$\overline{u_2} = \frac{1}{2b}\int_{-b}^{b} u_{200}(z)\mathrm{d}z, \tag{87}$$

where $u_{200}(z)$ is given by (76)–(78). Thus, (79) becomes

$$\overline{u} \simeq b^2 \left(\frac{1}{3} + \frac{\varepsilon^2}{4} G_0 \right) + \varepsilon^2 \overline{u_2}. \tag{88}$$

Substitution of (76)–(78) into (87) yields

$$\overline{u_2} = \frac{1}{2}[u_{200}(b) + u_{200}(-b)] + \frac{\mathcal{R}}{4b} \int_{-b}^{b} (\tau^2 - b^2) F(\tau) \mathrm{d}\tau. \tag{89}$$

Ultimately, the average velocity is calculated up to $O(\varepsilon^3)$ by

$$\overline{u'} \simeq \frac{1}{3} b'^2 + \varepsilon^2 h(\mathcal{R}), \tag{90}$$

where the dimensionless function $h(\mathcal{R})$ has the form

$$h(\mathcal{R}) = -\frac{b'^2 G_0}{4} + \frac{1}{2}[u'_{200}(b') + u'_{200}(-b')] + \frac{\mathcal{R}}{2b'} \int_{-b'}^{b'} (\tau^2 - b'^2) F(\tau) \mathrm{d}\tau \tag{91}$$

and $F(\tau)$, $u_{200}(b)$ and $u_{200}(-b)$ are expressed by (75) and by (77), respectively, in terms of the Fourier coefficients of the first-order approximation $\mathbf{u}_1(x, y, z)$ calculated in Sect. 4.2 and of the known functions $T(x, y)$ and $B(x, y)$.

5 Forchheimer's law up to $O(\varepsilon^3)$

5.1 Analytical form of the law

Following the general method described in Sect. 2, write Eq. (90) in the form (compare to (27))

$$\overline{u^*} = |\overline{\nabla p^*}| \left[\frac{1}{3} b'^2 + \varepsilon^2 h\left(\mathcal{R}_{\mathrm{loc}} |\overline{\nabla p^*}| \right) \right]. \tag{92}$$

In order to construct the dependence $|\overline{\nabla p^*}|$ on $\overline{u^*}$, it is convenient to introduce the variables

$$X = \mathcal{R}_{\mathrm{loc}} |\overline{\nabla p^*}|, \quad Y = \mathcal{R}_{\mathrm{loc}} \overline{u^*}. \tag{93}$$

Then, (92) becomes

$$Y = X \left[\frac{b'^2}{3} + \varepsilon^2 h\,(X) \right]. \tag{94}$$

All calculations in this section are performed with the accuracy $O(\varepsilon^2)$. Hence, the inverse function $X = X(Y)$ should be calculated with the same accuracy:

$$X(Y) = X_0(Y) + \varepsilon^2 X_1(Y). \tag{95}$$

Substitute (95) into (94) and take the coefficients of ε^0 and of ε^2

$$Y = \frac{b'^2}{3} X_0, \quad \frac{b'^2}{3} X_1 + X_0 h(X_0) = 0. \tag{96}$$

This system has the solution

$$X_0 = \frac{3}{b'^2} Y, \quad X_1 = -Y \left(\frac{3}{b'^2} \right)^2 h\left(\frac{3}{b'^2} Y \right). \tag{97}$$

Substitution of (93) into (97) and (95) yields the required dependence

$$|\overline{\nabla p^*}| = \frac{3}{b'^2}\overline{u^*}\left[1 - \varepsilon^2 \frac{3}{b'^2} h\left(\frac{3}{b'^2}\mathcal{R}_{\rm loc}\overline{u^*}\right)\right]. \tag{98}$$

This is the nonlinear Darcy's flow to $O(\varepsilon^2)$ for the channel bounded by the walls (101). The performed calculations give reasonable results at least for $\mathcal{R} < 10^9$. A rational approximation in ε of the function (94) can be taken as

$$X = \frac{3}{b'^2} Y \left[1 + \varepsilon^2 \frac{3}{b'^2} h\left(\frac{3}{b'^2} Y\right)\right]^{-1}. \tag{99}$$

The rational approximation (99) in ε is taken for the following reasons. It was established in [15] that the ε expansions (54) converge if

$$\varepsilon < \varepsilon_c = \left[b \sup_{s,t}\left(a_{st} \max\left(\sqrt{s^2+t^2}, \sqrt{\mathcal{R}_e\sqrt{s^2+t^2}}\right)\right)\right]^{-1}, \tag{100}$$

where a_{st} is the maximal modulus from eight coefficients of $\exp i(\pm sx \pm ty)$ in the double complex Fourier series of $2T(x, y)$ and $2B(x, y)$. Therefore, (98) holds for ε satisfying (100) and (99) holds for greater ε. [16] showed that such Padé approximations can be valid for much greater values than ε_c.

5.2 Example and decomposition into intervals

Below, all numerical calculations are applied to the two-dimensional channel with the walls

$$z' = \pm b'[1 + \varepsilon \cos(x')], \tag{101}$$

where again dimensional and dimensionless values are distinguished by primes as said in Sect. 2. (42) corresponds to $b' = 1$. Each calculation is performed for a fixed Reynolds number $\mathcal{R}$. The algorithm can be easily applied to other channels.

Investigate the function (91) for the channel (101) given as a numerical table after the numerical solution to the problem (59)–(60). Its behaviour for all Reynolds numbers ($\mathcal{R} \leqslant 10^8$) with $b' = 1$ is shown in Fig. 1 and is detailed in Figs. 3, 4, 5. As one can see later, the function $h(\mathcal{R})$ plays a key role in the nonlinear Darcy law up to $O(\varepsilon^3)$.

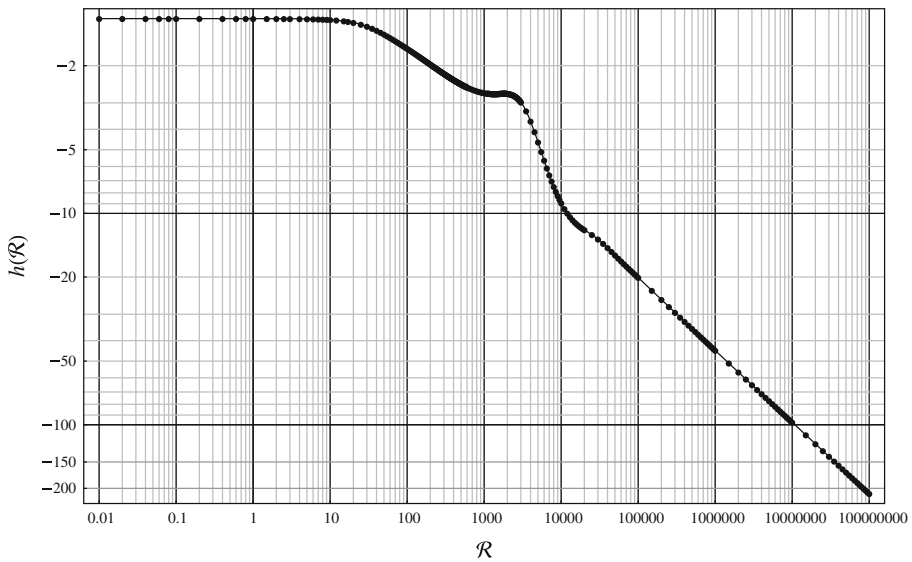

Fig. 1 The computed function $h(\mathcal{R})$ for the channel (101) when $\mathcal{R} \leq 10^8$

We now proceed to investigate the curve $h = h(\mathcal{R})$ using various Padé approximations. It is possible to take an approximation for all $\mathcal{R}$. However, better approximations of $h = h(\mathcal{R})$ are obtained when specific formulae are calculated for various intervals of $\mathcal{R}$.

When different Padé approximations are applied to the data on the segment $(0, \mathcal{R}_{\max})$ for a variable $\mathcal{R}_{\max}$, one can note that the minimal pole of the approximations stabilizes near the point $\mathcal{R} = -58i$ where $i = \sqrt{-1}$. The different Padé approximations yield almost the same numerical results up to $\mathcal{R} = 1{,}000$. An approximation of order (6, 6) has the form

$$h = \frac{-1.19787 - 5.54757 \times 10^{-4}\mathcal{R}^2 - 2.42030 \times 10^{-8}\mathcal{R}^4 - 1.37449 \times 10^{-13}\mathcal{R}^6}{1 + 3.42315 \times 10^{-4}\mathcal{R}^2 + 1.13784 \times 10^{-8}\mathcal{R}^4 + 4.85751 \times 10^{-14}\mathcal{R}^6} \tag{102}$$

It is obtained for $\mathcal{R}_{\max} = 300$; the closest pole to zero is $\mathcal{R} = -57.2033i$. It is worth noting that all the coefficients impact on h because of large numbers $\mathcal{R}^6$. For instance, the term $4.85751 \times 10^{-14}\, R^6 \approx 35.4$ for $\mathcal{R} = 300$.

Consider another approximation of order (6, 6) with $\mathcal{R}_{\max} = 550$

$$h = \frac{-1.19798 - 5.41188 \times 10^{-4}\mathcal{R}^2 - 2.15115 \times 10^{-8}\mathcal{R}^4 - 1.05405 \times 10^{-13}\mathcal{R}^6}{1 + 3.31697 \times 10^{-4}\mathcal{R}^2 + 9.92225 \times 10^{-9}\mathcal{R}^4 + 3.68731 \times 10^{-14}\mathcal{R}^6} \tag{103}$$

The closest pole to zero has almost the same value $\mathcal{R} = -57.1192i$.

Figure 1 shows that the curve $h = h(\mathcal{R})$ has different behaviour on segments $I_1 = (0,\ 500)$, $I_2 = (500,\ 3 \times 10^4)$, $I_3 = (3 \times 10^4,\ 10^8)$. This division into three segments is of course arbitrary.

5.2.1 Behaviour of h in I_1

For instance, h is well approximated by a quadratic polynomial (see Fig. 2)

$$h = -1.19804 - 1.33153 \times 10^{-4}\mathcal{R}^2 \quad \text{in } I_{11} = (0, 12). \tag{104}$$

For $\mathcal{R} > 12$, other powers of $\mathcal{R}$ have to be taken into account. However, the first segment can be extended to $\mathcal{R} = 1{,}000$ since formulae (102)–(103) correspond to the data with high precision up to $\mathcal{R} = 1{,}000$. I_1 contains the characteristic point near $\mathcal{R} = -57.2i$ where the functions (102) and (103) have a pole. This implies that the radius of convergence of the Taylor series in powers of $\mathcal{R}$ is equal to 57.2. It is known [23] that the problem (18)–(20) has a unique solution for sufficiently small $\mathcal{R}$. Our computations imply that this unique solution holds at least for $\mathcal{R} < 57.2$. As a consequence, Forchheimer's law has a cubic correction for such Reynolds numbers. Computations demonstrate that the data can be approximated by an even function $h(\mathcal{R})$ on the whole segment I_1. A further increase in $\mathcal{R}$ would lead to a polynomial approximation for $h(\mathcal{R})$. It is difficult to say whether it is the effect of transformation of $h(\mathcal{R})$ from an even to a general function. Actually, any finite data can be approximated by an even function.

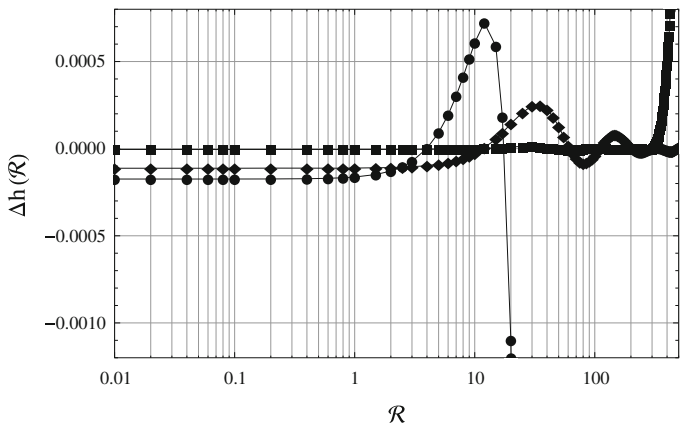

Fig. 2 Fitting residuals for small Reynolds numbers $0 \leqslant \mathcal{R} \leqslant 500$: (104) *dots*; (102) *squares*; (103) *diamonds*

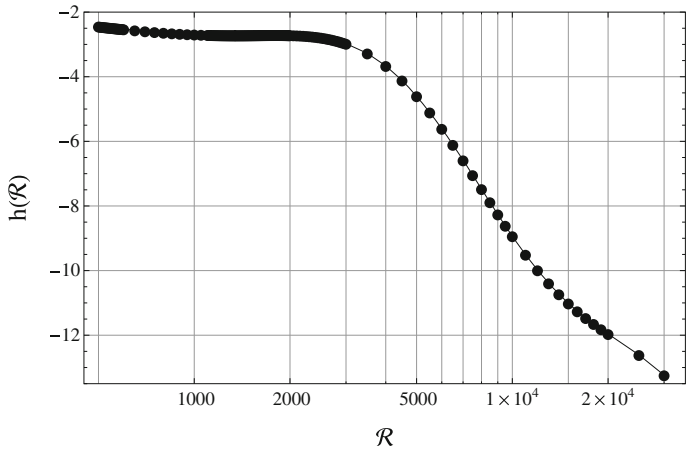

Fig. 3 The computed function $h(\mathcal{R})$ for intermediate Reynolds numbers $500 \leqslant \mathcal{R} \leqslant 30{,}000$

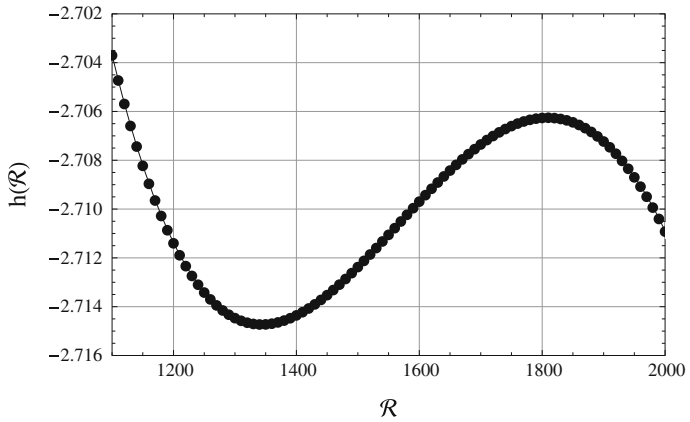

Fig. 4 Local extrema of $h(\mathcal{R})$ on segment $1{,}100 \leqslant \mathcal{R} \leqslant 2{,}000$

5.2.2 Behaviour of h in I_2

The behaviour of $h = h(\mathcal{R})$ in I_2 is illustrated in Fig. 3. Here, the function $h(\mathcal{R})$ has two local extrema, namely a local minimum $h_{\min} = -2.71470$ at $\mathcal{R} = 1{,}340$ and a local maximum $h_{\max} = -2.70623$ at $\mathcal{R} = 1{,}810$ (see Fig. 4). Therefore, the function $h(\mathcal{R}_e)$ decreases everywhere except in the segment (1,340, 1,810). The function $h(\mathcal{R})$ slowly changes in the segment (900, 3,000) and can be approximated here by the constant -2.5 (see Fig. 3). This means that $|\overline{\nabla p^*}|$ decreases with the average velocity $\overline{u^*}$ everywhere except for $1{,}340 < \frac{3}{b'^2}\mathcal{R}_{\text{loc}}\overline{u^*} < 1{,}810$ [see (98)] where $|\overline{\nabla p^*}|$ increases. To the best of our knowledge, this effect was not noted experimentally and theoretically in the previous investigations.

5.2.3 Behaviour of h in I_3

In the segment I_3 when $\mathcal{R} > 30{,}000$, the data are perfectly approximated by the power function (see Fig. 5)

$$h = 1.11310 - 0.458092\sqrt[3]{\mathcal{R}}. \tag{105}$$

For the channel (101), $\varepsilon_c = \left(b\sqrt{\mathcal{R}_e}\right)^{-1}$. In order to avoid the restrictions (100), it is possible to use Padé approximations as it was demonstrated in [15,16]. Hence, formula (99) extends (98) to larger values of ε.

Substitution of (105) into (98) and (99) implies, respectively, the following formulae valid up to ε^3:

$$|\overline{\nabla p^*}| = \frac{3}{b'^2}\overline{u^*}\left[1 - \varepsilon^2\frac{3}{b'^2}\left(1.1131 - 0.458092\sqrt[3]{\frac{3}{b'^2}\mathcal{R}_{\text{loc}}\overline{u^*}}\right)\right] \tag{106}$$

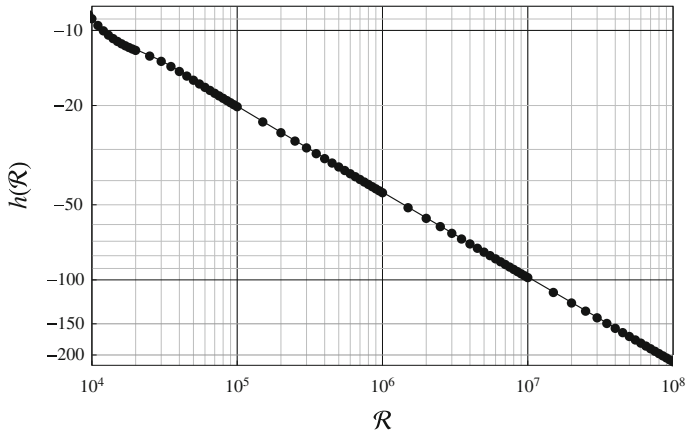

Fig. 5 Computed data $h(\mathcal{R})$ for large Reynolds numbers $\mathcal{R} \geqslant 30{,}000$

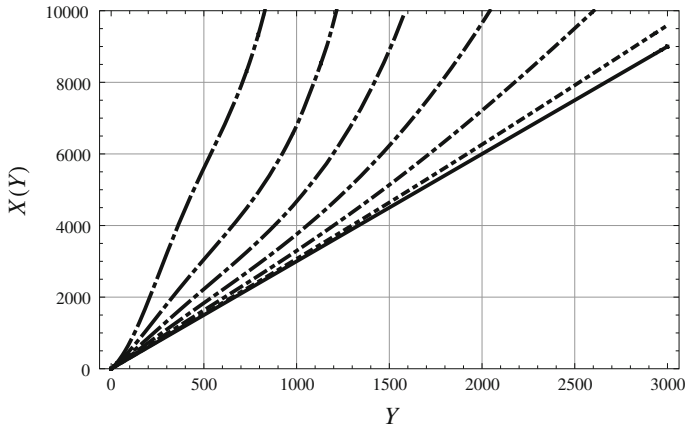

Fig. 6 The function $X(Y)$ (99). Data are for $b' = 1$; ε: 0 *solid*; 0.05 ···; 0.10 - ·· - ; 0.15 – ·– ; 0.20 — ·— ; 0.25 —— ·—— ; 0.30 —— · ——

and

$$|\overline{\nabla p^*}| = \frac{3}{b'^2}\overline{u^*}\left[1 + \varepsilon^2\frac{3}{b'^2}\left(1.1131 - 0.458092\sqrt[3]{\frac{3}{b'^2}\mathcal{R}_{\mathrm{loc}}\overline{u^*}}\right)\right]^{-1}. \tag{107}$$

The first formula (106) is valid for small $\varepsilon < b'$. The second formula (107) holds for $\varepsilon > b'$ and for not large $\mathcal{R}_{\mathrm{loc}}$. One can take $\mathcal{R}_{\mathrm{loc}} \to +\infty$ in (106) and obtain the asymptotic formula valid for large $\mathcal{R}_{\mathrm{loc}}$ (compare to (7) from [14])

$$|\overline{\nabla p^*}| = 6\varepsilon^2 b'^{-\frac{14}{3}}\mathcal{R}_{\mathrm{loc}}^{\frac{1}{3}}\overline{u^*}^{\frac{4}{3}}. \tag{108}$$

The difference between the nonlinear and the linear Darcy laws is shown in Fig. 6.

5.3 Different forms of the Forchheimer's law for different $\mathcal{R}$

The Reynolds numbers plays a fundamental role in the behaviour of viscous fluids as it is demonstrated by numerous physical experiments. Theoretical scales of the Reynolds numbers are based on its critical value $\mathcal{R}$ from which turbulent flow begins.

We propose another type of rigorous mathematical scales in order to describe stationary flow in porous media. From a physical point of view, the scales correspond to different behaviours of fluid. Forchheimer's

law $\left|\overline{\nabla p^*}\right| = G(\mathcal{R}_{\rm loc}, \overline{u^*})$ can be considered as a function of $\overline{u_c^*}$ where the function G may have different expressions which depend on the parameter $\mathcal{R}_{\rm loc}$.

In order to relate our results with others, it is necessary to take an adequate characteristic velocity U_0 in the definition (25a) of $\mathcal{R}_{\rm loc}$. Usually, U_0 is taken as the central velocity in the straight channel [24], i.e., when $\varepsilon = 0$

$$U_0 = \frac{|\nabla p|\, b^2}{2\mu}. \tag{109}$$

Then, (25a) yields

$$\mathcal{R}_{\rm loc} = \frac{\rho\, |\nabla p|\, b^2 l}{2\mu^2}$$

and (5) implies that

$$\frac{\mathcal{R}_{\rm loc}}{\mathcal{R}} = \frac{1}{2}\left(\frac{b}{l}\right)^2. \tag{110}$$

Using the dimensionless parameter $b' = b/l$, we obtain

$$\frac{\mathcal{R}_{\rm loc}}{b'^2} = \frac{1}{2}\mathcal{R}. \tag{111}$$

Note that the choice of U_0 is convenient since it does not depend on ϵ. Instead of (109), one could take another value of U_0 which would yield another coefficient in (111) and another scale in Fig. 7.

The numerical results of Sect. 5.2 for the channel (101) suggest the following scales for the Reynolds numbers $\mathcal{R}_{\rm loc}$ illustrated in Fig. 7.

The following approximate Reynolds numbers are marked:

$0 \le \mathcal{R}_{\rm loc} \le 6$: quadratic approximation (104) for $h(\mathcal{R})$.
$0 \le \mathcal{R}_{\rm loc} \leqslant 28$: convergence domain for the Taylor series in $\mathcal{R}_{\rm loc}$.
$0 \le \mathcal{R}_{\rm loc} \leqslant 250$: approximation of $h(\mathcal{R})$ by an even function.
$450 \leqslant \mathcal{R}_{\rm loc} \leqslant$ 1,500: weak dependence of $\left|\overline{\nabla p^*}\right|$ on the velocity.
$\mathcal{R}_{\rm loc} \geqslant$ 15,000: the power law (108).

The Reynolds numbers derived from the stability theory are also given (see [4,5,24] and others); the following critical values are marked:

$\mathcal{R}_{\rm loc}$ of order 100 for curvilinear channels [25,26].
$\mathcal{R}_{\rm loc}$ of order 1,000: spatial stability.
$\mathcal{R}_{\rm loc} = 5{,}772$: plane stability.
$2{,}300 \le \mathcal{R}_{\rm loc} \le 50{,}000$: transition to turbulence.

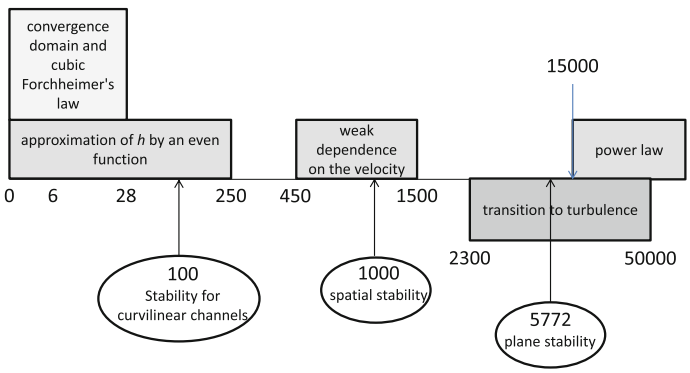

Fig. 7 Scale of Reynolds numbers $\mathcal{R}_{\rm loc} = \frac{1}{2}\mathcal{R}$. Known stability results are also indicated

This diagram for Forchheimer's law (98) with $b' = 1$ is based on the function $h(\mathcal{R})$ shown in Fig. 1. The cubic law is obtained from (98) by substitution of (104) and the "odd law" by substitution of (102) or (103).

Experimental results for different step channels were obtained by [10]. The cubic Forchheimer's law is shown to hold up to $\mathcal{R}_{\rm loc} \sim 20-70$ and it becomes a quadratic law for greater $\mathcal{R}_{\rm loc}$ (see Fig. 7). This corresponds to our results for the channel (101) when the Taylor series converges up to $\mathcal{R}_{\rm loc} = 28$. Theoretically, this value can be considered as the critical one up to which the cubic law holds for sinusoidal channels. Moreover, above $\mathcal{R}_{\rm loc} = 100$, the flow becomes unstable [25] and this should disturb the theoretical cubic law.

The theoretical justification of the radical change from the cubic to the quadratic dependence in Forchheimer's law follows from different rational approximations of the function $h(\mathcal{R})$ depending on the complex variable $\mathcal{R}$. Let $\mathcal{R}_1$ and $\mathcal{R}_2$ be complex singularities of the function $h(\mathcal{R})$ which are closest to zero and $|\mathcal{R}_1| < |\mathcal{R}_2|$. Then, $h(\mathcal{R})$ can be represented by a Taylor series in the complex disk $|\mathcal{R}| < |\mathcal{R}_1|$ and in the annulus $|\mathcal{R}_1| < |\mathcal{R}| < |\mathcal{R}_2|$ by a Laurent series. Of course, these two representations of the same function $h(\mathcal{R})$ analytic in two disjoint domains have different structures. In particular, the function $h(\mathcal{R})$ can be approximated by polynomials in the real segment $|\mathcal{R}_1| < \mathcal{R} < |\mathcal{R}_2|$ which corresponds to the quadratic Forchheimer's law. The scales in Fig. 7 correspond to complex singularities of $h(\mathcal{R})$ that justify different analytic representations of Forchheimer's law for different Reynolds numbers.

6 Conclusion

The main result of this paper is that there is no quadratic correction to Darcy's law for small $\mathcal{R}$, but that there is one for large $\mathcal{R}$. This result is proved by the application of two different analytical–numerical algorithms to the full Navier–Stokes equations. The first method described in Sect. 3 is based on the double expansion in ε and in the Reynolds number $\mathcal{R}$ defined by (5); hence, it is valid for sufficiently small $\mathcal{R}$. A theoretical investigation of the method applied to channels bounded by symmetric walls leads to "the odd law" (41) which yields the cubic dependence (6). All the examples including various non-symmetric channels presented in Sect. 3.3 and [11] confirm this assertion.

The second method is based on the ε expansion and formally holds for practically arbitrary $\mathcal{R}$. The final formula (92) expresses the nonlinear Darcy law where the deviation of the linear term is described by the numerically calculated function h given by (91).

Stability and transition to turbulence are not studied here; known results [4,5,24–27] are put in Fig. 7 under the axis $R_{\rm loc}$. Our results concern the nonlinear Darcy flow which are above the axis $R_{\rm loc}$. The results of the various regimes for nonlinear Darcy flow and stability were not compared in previous works. From a mathematical point of view, the question is stated as follows: are the domains of inverse stationary flow (Moffat's eddies) and the bifurcation points (in terms of the Reynolds number) related to stability of the non-stationary Navier–Stokes equations. It should be noted that physicists frequently confuse Moffat's eddies and turbulence. Our previous results [15] suggest that Moffat's eddies are not related to turbulence while the bifurcation points perhaps are related to them. However, this is only a qualitative observation.

As is pointed out above, it is not known which relation is valid between the characteristic parameters of the stationary and non-stationary flows for $\mathcal{R} \sim 3{,}200$–$50{,}000$ (transition to turbulence observed in various cases) and for $\mathcal{R} \sim 5{,}772$ for plane channels. As was demonstrated in [15], domains of inverse stationary flow (Moffat's eddies) roughly speaking increase with the Reynolds number. The effect of turbulence for $\mathcal{R} \sim 3{,}200$–$50{,}000$ means that the flow changes unpredictably in time by change of the domains of inverse flow (structure of the flow). There are many possible scenarios of such flows, but their structures are similar to a mixture of vortices [27]. Our description of the flow for any $\mathcal{R}$ is one of the many possible scenarios of the non-stationary flows beyond stability.

The nonlinear Darcy flow is obtained through the average velocity. It was shown in [15,16] that the local velocity for stationary flows essentially depends on eddies while the average velocity weakly depends on eddies. This suggests that the average velocity does not drastically change in various scenarios for $\mathcal{R} \sim 50{,}000$. Thus, the average velocity of one flow described in our paper for any Reynolds number can possibly correspond to the average velocity of all possible flows. So, one scenario is discussed here up to $\mathcal{R} = \infty$ among many possible scenarios and this scenario is thought to be typical.

This paper could be extended in many ways, but the most important is certainly the analysis of bifurcations and the stability of the solutions which were obtained and their influence on the nonlinear Darcy law.

7 Appendix: Proof of (41)

7.1 Structure of the solution of the primary problem

In the present section, the structure of the primary problem which has to be solved at each step of the cascades in $\mathcal{R}$ and ε is studied. Consider the equations

$$\begin{aligned} &\nabla^2 \mathbf{v} = \nabla q + \mathbf{F}, \\ &\nabla \cdot \mathbf{v} = 0 \end{aligned} \tag{112}$$

in $-b < z < b$ with the boundary conditions

$$\mathbf{v}(x, y, b) = \mathbf{f}(x, y), \quad \mathbf{v}(x, y, -b) = \mathbf{g}(x, y). \tag{113}$$

Lemma 1 *Let* $\mathbf{v} = (v_1, v_2, v_3)$ *and the given functions* $\mathbf{F} = (\mathcal{F}_1, \mathcal{F}_2, \mathcal{F}_3), \mathbf{f} = (f_1, f_2, f_3), \mathbf{g} = (g_1, g_2, g_3)$ *satisfy the following conditions as functions of* x *and* y*:*

(i) $\mathcal{F}_1, \mathcal{F}_2, f_1, f_2, g_1, g_2$ *are even,* $\mathcal{F}_3, f_3, g_3$ *are odd. Then,* v_1, v_2 *are even and* v_3 *is odd.*
(ii) $\mathcal{F}_1, \mathcal{F}_2, f_1, f_2, g_1, g_2$ *are odd and* $\mathcal{F}_3, f_3, g_3$ *are even. Then,* v_1, v_2 *are odd and* v_3 *is even.*

Proof Let $\mathcal{F}_1, \mathcal{F}_2, f_1, f_2, g_1, g_2$ be even functions of x and y, and $\mathcal{F}_3, f_3, g_3$ be odd. Then, they are represented as Fourier series

$$\begin{aligned} \mathcal{F}_1(x, y, z) &= \sum_{s,t=0}^{\infty} \mathcal{F}_1^{(s,t)}(z) \cos sx \cos ty, \quad \mathcal{F}_2(x, y, z) = \sum_{s,t=0}^{\infty} \mathcal{F}_2^{(s,t)}(z) \cos sx \cos ty, \\ \mathcal{F}_3(x, y, z) &= \sum_{s,t=1}^{\infty} \mathcal{F}_3^{(s,t)}(z) \sin sx \sin ty, \\ f_1(x, y) &= \sum_{s,t=0}^{\infty} f_1^{(s,t)} \cos sx \cos ty, \quad f_2(x, y) = \sum_{s,t=0}^{\infty} f_2^{(s,t)} \cos sx \cos ty, \\ f_3(x, y) &= \sum_{s,t=1}^{\infty} f_3^{(s,t)} \sin sx \sin ty, \\ g_1(x, y) &= \sum_{s,t=0}^{\infty} g_1^{(s,t)} \cos sx \cos ty, \quad g_2(x, y) = \sum_{s,t=0}^{\infty} g_2^{(s,t)} \cos sx \cos ty, \\ g_3(x, y) &= \sum_{s,t=1}^{\infty} g_3^{(s,t)} \sin sx \sin ty. \end{aligned} \tag{114}$$

The problem (112)–(113) can be solved by separation of variables. Fix a wave vector (s, t) with non-zero components. The case $s = 0$ or (and) $t = 0$ is considered in the same way. Consider the following special problem

$$\begin{aligned} &\nabla^2 \mathbf{U}_{st} = \nabla Q_{st} + \left(\mathcal{F}_1^{(st)}(z) \cos sx \cos ty, \mathcal{F}_2^{(st)}(z) \cos sx \cos ty, \mathcal{F}_3^{(st)}(z) \sin sx \sin ty\right), \\ &\nabla \cdot \mathbf{U}_{st} = 0 \end{aligned} \tag{115}$$

in $-b < z < b$ with the boundary conditions

$$\begin{aligned} \mathbf{U}_{st}(x, y, b) &= \left(f_1^{(st)}(x, y), f_2^{(st)}(x, y), f_3^{(st)}(x, y)\right), \\ \mathbf{U}_{st}(x, y, -b) &= \left(g_1^{(st)}(x, y), g_2^{(st)}(x, y), g_3^{(st)}(x, y)\right). \end{aligned} \tag{116}$$

This problem has a unique solution up to an additive constant in $Q_{(st)}$ as a boundary value problem for the Stokes equations. We now demonstrate that $\mathbf{U}_{(st)}$ and $Q_{(st)}$ can be constructed in the form

$$\begin{aligned}\mathbf{U}_{st}(x,y,z) &= (\alpha_{st}(z)\cos sx\cos ty, \beta_{st}(z)\cos sx\cos ty, \gamma_{st}(z)\sin sx\sin ty),\\ Q_{st}(x,y,z) &= \delta_{st}(z)\sin sx\sin ty.\end{aligned} \tag{117}$$

Substitution of (117) into (115) yields the ordinary differential equations

$$\begin{aligned}&\alpha_{st}''(z) - (s^2+t^2)\alpha_{st}(z) - \delta_{st}(z) = \mathcal{F}_1^{(st)}(z),\\ &\beta_{st}''(z) - (s^2+t^2)\beta_{st}(z) - \delta_{st}(z) = \mathcal{F}_2^{(st)}(z),\\ &\gamma_{st}''(z) - (s^2+t^2)\gamma_{st}(z) - \delta_{st}'(z) = \mathcal{F}_3^{(st)}(z),\\ &\gamma_{st}'(z) - s\alpha_{st}(z) - t\beta_{st}(z) = 0.\end{aligned} \tag{118}$$

Substitution of (117) and (114) into (116) yields the boundary conditions

$$\alpha_{st}(b) = f_1^{(st)}, \alpha_{st}(-b) = g_1^{(st)}, \beta_{st}(b) = f_2^{(st)}, \beta_{st}(-b) = g_2^{(st)}, \gamma_{st}(b) = f_3^{(st)}, \gamma_{st}(-b) = g_3^{(st)}. \tag{119}$$

The problem (118)–(119) has been solved in [15,16]. Exact formulae for $\alpha_{st}(z)$, $\beta_{st}(z)$ and $\gamma_{st}(z)$ were written and are not repeated here. Then, $\mathbf{U}_{st}(x,y,z)$ has the form (117) and

$$\mathbf{v}(x,y,z) = \sum_{s,t=0}^{\infty} (\alpha_{st}(z)\cos sx\cos ty, \beta_{st}(z)\cos sx\cos ty, \gamma_{st}(z)\sin sx\sin ty)\,. \tag{120}$$

$v_1(x,y,z)$ and $v_2(x,y,z)$ are seen to be even functions in x and y while $v_3(x,y,z)$ is odd in these two variables.

The second part of the lemma is proved by the same method. □

7.2 Structure of the cascade and of its solutions

In the present section, Lemma 1 is applied to the cascade (33)–(34). First, consider the zeroth problem (33) which is reduced to the following cascade in ε. The partial differential equations are given in the layer $-b < z < b$ by

$$\begin{aligned}\nabla^2\mathbf{u}_m^{(0)} &= \nabla p_m^{(0)},\\ \nabla\cdot\mathbf{u}_m^{(0)} &= 0,\end{aligned} \tag{121}$$

with the boundary conditions

$$\begin{aligned}\mathbf{u}_m^{(0)}(x,y,b) &= -\sum_{n=1}^{m}\frac{(bT)^n}{n!}\frac{\partial^n\mathbf{u}_{m-n}^{(0)}}{\partial z^n}(x,y,b),\\ \mathbf{u}_m^{(0)}(x,y,-b) &= -\sum_{n=1}^{m}\frac{(bB)^n}{n!}\frac{\partial^n\mathbf{u}_{m-n}^{(0)}}{\partial z^n}(x,y,-b).\end{aligned} \tag{122}$$

The zeroth solution $\mathbf{u}_0^{(0)}$, $p_0^{(0)}$ has the form (36).

Lemma 2 *Let* $\mathbf{u}_m^{(0)} = (u_m^{(0)}, v_m^{(0)}, w_m^{(0)})$ *be the solutions of the cascade* (121)–(122). *Then,* $u_m^{(0)}, v_m^{(0)}$ *are even, and* $w_m^{(0)}$ *odd in* x *and* y *for all* $m = 0, 1, 2, \ldots$.

Proof It is based on the principle of induction on m. The functions $u_0^{(0)} = b^2 - z^2$, $v_0^{(0)} = 0$ are even functions of x and y; $w_0^{(0)} = 0$ is odd. Let us assume that the same is true for $u_n^{(0)}$, $v_n^{(0)}$ and $w_n^{(0)}$ $(n = 1, 2, \ldots, m-1)$ and let us prove it for $n = m$. Consider the right hand sides of the boundary conditions (122). The differentiation on z of $\mathbf{u}_n^{(0)}(x, y, z)$ $(n = 1, 2, \ldots, m-1)$ does not change the evenness of $u_n^{(0)}(x, y, z)$, $v_n^{(0)}(x, y, z)$ and oddness of $w_n^{(0)}(x, y, z)$ in x and y. Since $T(x, y)$ and $B(x, y)$ are even, $u_m^{(0)}(x, y, \pm b)$ and $v_m^{(0)}(x, y, \pm b)$ are even while $w_m^{(0)}(x, y, \pm b)$ is odd. Then, Lemma 1 implies that $u_m^{(0)}(x, y, z)$ and $v_m^{(0)}(x, y, z)$ are even while $w_m^{(0)}(x, y, z)$ is odd.

The lemma is proved. □

Since $\mathbf{u}^{(0)}$ is a sum of $\mathbf{u}_m^{(0)}$, Lemma 2 implies the following

Corollary 1 *Let* $\mathbf{u}^{(0)} = (u^{(0)}, v^{(0)}, w^{(0)})$. *Then,* $u^{(0)}(x, y, z)$ *and* $v^{(0)}(x, y, z)$ *are even in* x *and* y *while* $w^{(0)}(x, y, x)$ *is odd.*

Lemma 3 *Let* $\mathbf{u}^{(k)} = (u^{(k)}, v^{(k)}, w^{(k)})$ *be solutions of the cascade* (34). *Then,* $u^{(k)}(x, y, z)$, $v^{(k)}(x, y, z)$ *are even on* x *and* y, $w^{(k)}(x, y, x)$ *is odd for even numbers* k; $u^{(k)}(x, y, z)$, $v^{(k)}(x, y, z)$ *are odd,* $w^{(k)}(x, y, x)$ *is even for odd numbers* k.

Proof Let $\mathbf{u}^{(k)} = (u^{(k)}, v^{(k)}, w^{(k)})$ and $\mathbf{u}^{(k+1)} = (u^{(k+1)}, v^{(k+1)}, w^{(k+1)})$ be solutions of two successive problems of the cascade (34). It follows from Corollary 3 that $u^{(0)}$ and $v^{(0)}$ are even while $w^{(0)}$ is odd. To prove the lemma, it is sufficient to demonstrate that the transformation $\mathbf{u}^{(k)} \mapsto \mathbf{u}^{(k+1)}$ maps even components to odd ones and vice versa. This property will be shown by induction on k.

At the beginning, $u^{(1)}$ and $v^{(1)}$ are proved to be odd and $w^{(1)}$ even, i.e., the induction assumption is verified for $k = 0$. Consider (34) with $k = 1$

$$\begin{aligned} \nabla^2 \mathbf{u}^{(1)} &= \nabla p^{(1)} + \mathbf{F}^{(1)}, \\ \nabla \cdot \mathbf{u}^{(1)} &= 0, \end{aligned} \tag{123}$$

where

$$\mathbf{F}^{(1)} = (\mathcal{F}_1, \mathcal{F}_2, \mathcal{F}_3) = (\mathbf{u}^{(0)} \cdot \nabla)\mathbf{u}^{(0)}, \tag{124}$$

$$\begin{aligned} \mathcal{F}_1 &= u^{(0)} \frac{\partial u^{(0)}}{\partial x} + v^{(0)} \frac{\partial u^{(0)}}{\partial y} + w^{(0)} \frac{\partial u^{(0)}}{\partial z}, \\ \mathcal{F}_2 &= u^{(0)} \frac{\partial v^{(0)}}{\partial x} + v^{(0)} \frac{\partial v^{(0)}}{\partial y} + w^{(0)} \frac{\partial v^{(0)}}{\partial z}, \\ \mathcal{F}_3 &= u^{(0)} \frac{\partial w^{(0)}}{\partial x} + v^{(0)} \frac{\partial w^{(0)}}{\partial y} + w^{(0)} \frac{\partial w^{(0)}}{\partial z}. \end{aligned} \tag{125}$$

The functions $\mathcal{F}_1(x, y, z)$, $\mathcal{F}_2(x, y, z)$ are odd functions of x and y since all summands of the definition (125) of $\mathcal{F}_1(x, y, z)$ are odd. For instance, $u^{(0)}(x, y, z)$ is even and $\frac{\partial u^{(0)}}{\partial x}(x, y, z)$ is odd (as a derivative of an even function). Similar arguments yield that $\mathcal{F}_2(x, y, z)$ is odd and $\mathcal{F}_3(x, y, z)$ even.

The problem (123) is reduced to the cascade in ε (37)–(38) with $k = 1$:

$$\begin{aligned} &\nabla^2 \mathbf{u}_m^{(1)} = \nabla p_m^{(1)} + \mathbf{F}_m^{(1)}, \\ &\nabla \cdot \mathbf{u}_m^{(1)} = 0, \quad m = 0, 1, 2, \ldots \\ &\mathbf{u}_m^{(1)}(x, y, b) = -\sum_{n=1}^{m} \frac{(bT)^n}{n!} \frac{\partial^n \mathbf{u}_{m-n}^{(1)}}{\partial z^n}(x, y, b), \\ &\mathbf{u}_m^{(1)}(x, y, -b) = -\sum_{n=1}^{m} \frac{(-bB)^n}{n!} \frac{\partial^n \mathbf{u}_{m-n}^{(1)}}{\partial z^n}(x, y, -b), \end{aligned} \tag{126}$$

where (39) implies

$$\mathbf{F}^{(1)}(x, y, z) = \sum_{m=1}^{\infty} \mathbf{F}_m^{(1)}(x, y, z)\varepsilon^m. \tag{127}$$

$\mathbf{F}_0^{(1)} = (\mathbf{u}^{(0)} \cdot \nabla)\mathbf{u}^{(0)} = 0$ in accordance with (36). Let the vectorial function $\mathbf{F}_m^{(1)}(x, y, z)$ have the form $\mathbf{F}_m^{(1)} = (\mathcal{F}_{m1}^{(1)}(x, y, z), \mathcal{F}_{m2}^{(1)}(x, y, z), \mathcal{F}_{m3}^{(1)}(x, y, z))$. The functions $\mathcal{F}_{m1}^{(1)}(x, y, z)$ and $\mathcal{F}_{m2}^{(1)}(x, y, z)$ are odd, and $\mathcal{F}_{m3}^{(1)}(x, y, z))$ even for all $m = 1, 2, \ldots$. The problem (126) for $m = 0$ has only the trivial solution since it is homogeneous ($\mathbf{F}_0^{(1)} = \mathbf{0}, \mathbf{u}_0^{(1)}(x, y, \pm b) = \mathbf{0}$ with a zero pressure jump).

The induction on k will include another induction on m. For instance, in order to check the required assertion for $k = 1$, it will be proved that $u_m^{(1)}(x, y, z)$ and $v_m^{(1)}(x, y, z)$ are odd and $w_m^{(1)}(x, y, z)$ even for all $m = 0, 1, 2, \ldots$ by induction on m. The trivial functions $u_0^{(1)}(x, y, z) \equiv 0, v_0^{(1)}(x, y, z) \equiv 0$ and $w_0^{(1)}(x, y, z) \equiv 0$ satisfy the required even–odd property. Let us assume that $u_n^{(1)}(x, y, z)$ and $v_n^{(1)}(x, y, z)$ are odd, and $w_n^{(1)}(x, y, z)$ even for $n = 1, 2, \ldots, m - 1$ and consider the next problem (126) with $n = m$. One can see that $u_n^{(1)}(x, y, \pm b)$ and $v_n^{(1)}(x, y, \pm b)$ are odd and $w_n^{(1)}(x, y, \pm b)$ even since $T(x, y)$ and $B(x, y)$ are even. Then, Lemma 1 implies that $u_m^{(1)}(x, y, z)$, $v_m^{(1)}(x, y, z)$ are odd and $w_m^{(1)}(x, y, z)$ even. Thus, the induction on m is completed. $u_m^{(1)}(x, y, z)$ and $v_m^{(1)}(x, y, z)$ are proved to be odd and $w_m^{(1)}(x, y, z)$ even for all $m = 0, 1, 2, \ldots$ The latter fact implies that $u^{(1)}(x, y, z)$ and $v^{(1)}(x, y, z)$ are odd while $w^{(1)}(x, y, z)$ is even. Therefore, the first step of the induction can be performed on k and the mapping $\mathbf{u}^{(0)} \mapsto \mathbf{u}^{(1)}$ satisfies the required property.

For definiteness, consider the mapping $\mathbf{u}^{(k)} \mapsto \mathbf{u}^{(k+1)}$ for even k, i.e., we assume that the functions $\mathbf{u}^{(0)}, \mathbf{u}^{(2)}, \ldots, \mathbf{u}^{(2p)}$ have even first and second components and odd third components; the functions $\mathbf{u}^{(1)}, \mathbf{u}^{(3)}, \ldots, \mathbf{u}^{(2p-1)}$ have odd first and second components and even third components. We now investigate $\mathbf{u}^{(2p+1)}$ satisfying (34) with $k = 2p + 1$:

$$\begin{aligned} \nabla^2 \mathbf{u}^{(2p+1)} &= \nabla p^{(2p+1)} + \mathbf{F}^{(2p+1)}, \\ \nabla \cdot \mathbf{u}^{(2p+1)} &= 0. \end{aligned} \tag{128}$$

By virtue of (39)

$$\mathbf{F}^{(2p+1)} = \left(\mathcal{F}_1^{(2p+1)}, \mathcal{F}_2^{(2p+1)}, \mathcal{F}_3^{(2p+1)}\right) = \sum_{n=0}^{2p} (\mathbf{u}^{(2p-n)} \cdot \nabla)\mathbf{u}^{(n)}, \tag{129}$$

where

$$\begin{aligned} \mathcal{F}_1^{(2p+1)} &= \sum_{n=0}^{2p} \left(u^{(2p-n)} \frac{\partial u^{(n)}}{\partial x} + v^{(2p-n)} \frac{\partial u^{(n)}}{\partial y} + w^{(2p-n)} \frac{\partial u^{(n)}}{\partial z} \right), \\ \mathcal{F}_2^{(2p+1)} &= \sum_{n=0}^{2p} \left(u^{(2p-n)} \frac{\partial v^{(n)}}{\partial x} + v^{(2p-n)} \frac{\partial v^{(n)}}{\partial y} + w^{(2p-n)} \frac{\partial v^{(n)}}{\partial z} \right), \\ \mathcal{F}_3^{(2p+1)} &= \sum_{n=0}^{2p} \left(u^{(2p-n)} \frac{\partial w^{(n)}}{\partial x} + v^{(2p-n)} \frac{\partial w^{(n)}}{\partial y} + w^{(2p-n)} \frac{\partial w^{(n)}}{\partial z} \right). \end{aligned} \tag{130}$$

The assumption of the induction implies that $\mathcal{F}_1^{(2p+1)}$ and $\mathcal{F}_2^{(2p+1)}$ are odd and $\mathcal{F}_3^{(2p+1)}$ even.

Equations (128) with zero boundary conditions are reduced to the cascade in ε

$$\begin{aligned} \nabla^2 \mathbf{u}_m^{(2p+1)} &= \nabla p_m^{(2p+1)} + \mathbf{F}_m^{(2p+1)}, \\ \nabla \cdot \mathbf{u}_m^{(2p+1)} &= 0, \quad m = 0, 1, 2, \ldots \\ \mathbf{u}_m^{(2p+1)}(x, y, b) &= -\sum_{n=1}^{m} \frac{(bT)^n}{n!} \frac{\partial^n \mathbf{u}_{m-n}^{(2p+1)}}{\partial z^n}(x, y, b), \\ \mathbf{u}_m^{(2p+1)}(x, y, -b) &= -\sum_{n=1}^{m} \frac{(-bB)^n}{n!} \frac{\partial^n \mathbf{u}_{m-n}^{(2p+1)}}{\partial z^n}(x, y, -b), \quad m = 0, 1, 2 \ldots \end{aligned} \tag{131}$$

Now, apply again the induction on m to (131) and demonstrate that $u_m^{(2p+1)}$ and $v_m^{(2p+1)}$ are odd and $w_m^{(2p+1)}$ even. It is true for $m = 0$ since $\mathbf{u}_0^{(2p+1)} = \mathbf{0}$. Let it be valid for $n = 0, 1, \ldots, m-1$. Check it for $n = m$. It follows from the boundary conditions (131) that $\mathbf{u}_m^{(2p+1)}(x, y, \pm b)$ has odd first and second coordinates and even third coordinates. Then, Lemma 1 implies that the same property holds for $\mathbf{u}_m^{(2p+1)}(x, y, z)$. The latter fact yields the required property for $\mathbf{u}^{(2p+1)}(x, y, z)$.

This completes the induction on m and subsequently on k; hence, the lemma is proved. □

We are interested in the average first component (24) of the velocity $\mathbf{u}(x, y, z)$ solving the problem (18)–(20). Substitution of (32) into (24) yields the expansion (recall that the primes are omitted for dimensionless values)

$$\overline{u} = \sum_{p=0}^{\infty} K_p \mathcal{R}^p, \tag{132}$$

where

$$K_p = \frac{1}{|\tau|} \int_{-\pi}^{\pi} \int_{-\pi}^{\pi} \mathrm{d}x\mathrm{d}y \int_{S^-(x,y)}^{S^+(x,y)} u^{(p)}(x, y, z)\mathrm{d}z. \tag{133}$$

Let us prove that $K_p = 0$ for odd p. It follows from Lemma 3 that $u^{(p)}(x, y, z)$ is odd in x and y. Then, the primitive in z

$$U^{(p)}(x, y, z) = \int u^{(p)}(x, y, z)\mathrm{d}z \tag{134}$$

is also odd in x and y. Then, the integral in (133)

$$V^{(p)}(x, y) = \int_{S^-(x,y)}^{S^+(x,y)} u^{(p)}(x, y, z)\mathrm{d}z = U^{(p)}[x, y, S^+(x, y)] - U^{(p)}[x, y, S^-(x, y)] \tag{135}$$

is an odd function in x and y because $U^{(p)}(x, y, z)$ is odd in the first and the second variables and $S^{\pm}(x, y)$ are even in x and y. Substitute the odd function $V^{(p)}(x, y)$ into (133). It is easily seen that

$$K_p = \frac{1}{|\tau|} \int_{-\pi}^{\pi} \int_{-\pi}^{\pi} V^{(p)}(x, y)\mathrm{d}x\mathrm{d}y = 0, \tag{136}$$

which justifies the odd expansion (41).

References

1. Adler, P.M.: Porous Media. Geometry and Transport. Butterworth-Heinemann, Stoneham (1992)
2. Forchheimer, P.: Wasserbewegung durch Boden. WDIZ **45**, 1782–1788 (1901)
3. Mei, C.C., Auriault, J.-L.: The effect of weak inertia on flow through a porous medium. J. Fluid Mech. **222**, 647–663 (1991)
4. Straughan, B.: Stability and Wave Motion in Porous Media. Springer Science+Business Media, LLC, Berlin (2008)
5. Straughan, B.: Explosive Instabilities in Mechanics. Springer, Heidelberg (1998)
6. Néel, M.C.: Convection forcée en milieu poreux: écarts à la loi de Darcy. C.R. Acad. Sci. Paris **326**, 615–620 (1998)
7. Payne, L.E., Straughan, B.: Unconditional nonlinear stability in temperature-dependent viscosity flow in a porous medium. Stud. Appl. Math. **105**, 59–81 (2000)
8. Wodie, J.-C., Levy, Th.: Correction non linéaire de la loi de Darcy. C. R. Acad. Sci. Paris Série II **312**, 157–161 (1991)
9. Skjetne, E., Auriault, J.-L.: New insights on steady, non-linear flow in porous medium. Eur. J. Mech. B/Fluid **18**, 131–145 (1999)
10. Cieslicki, K., Lasowska, A.: The first correction to the Darcy's law in view of the homogenization theory and experimental research. Arch. Mining Sci. **44**, 395–412 (1999)
11. Balhoff, M., Mikelić, A., Wheeler, M.F.: Polynomial filtration laws for low Reynolds number flows through porous media. Transport Porous Media **81**, 35–60 (2010)

12. Whitaker, S.: The Forchheimer equation: a theoretical development. Transp. Porous Media **25**, 27–61 (1996)
13. Chen, Z., Lyons, S.L., Qin, G.: Derivation of the Forchheimer law via homogenization. Transp. Porous Media **44**, 325–335 (2001)
14. Skjetne, E., Auriault, J.-L.: High-velocity laminar and turbulent flow in porous media. Transp. Porous Media **36**, 131–147 (1999)
15. Malevich, A.E., Mityushev, V.V., Adler, P.M.: Couette flow in channels with wavy walls. Acta Mech. **197**, 247–283 (2008)
16. Malevich, A.E., Mityushev, V.V., Adler, P.M.: Stokes flow through a channel with wavy walls. Acta Mechanica **182**, 151–182 (2006)
17. Scholle, M., Rund, A., Aksel, N.: Drag reduction and improvement of material transport in creeping films. Arch. Appl. Mech. **75**, 93–112 (2006)
18. Wierschem, A., Scholle, M., Aksel, N.: Vortices in film flow over strongly undulated bottom profiles at low Reynolds numbers. Phys. Fluids **15**, 426–435 (2003)
19. Heining, C., Pollak, T., Aksel, N.: Pattern formation and mixing in three-dimensional film flow. Phys. Fluids **24**, 042102 (2012)
20. Haas, A., Pollak, T., Aksel, N.: Side wall effects in thin gravity-driven film flow–steady and draining flow. Phys. Fluids **23**, 062107 (2011)
21. Pollak, T., Haas, A., Aksel, N.: Side wall effects on the instability of thin gravity-driven films—From long-wave to short-wave instability. Phys. Fluids **23**, 094110 (2011)
22. Shkalikov, A.A.: Spectral portraits of the Orr–Sommerfeld operator with large Reynolds numbers. Contemp. Math. Fundam. Dir. **3**, 89–112 (2003)
23. Galdi, G.P.: An Introduction to the Mathematical Theory of the Navier–Stokes Equations. Vol. II: Nonlinear Steady Problems. Springer, Berlin (1994)
24. Schmid, P.J., Henningson, D.S.: Stability and Transition in Shear Flows. Springer, Berlin (2001)
25. Szumbarski, J.: Instability of viscous incompressible flow in a channel with transversely corrugated walls. J. Theor. Appl. Mech. **45**, 659–683 (2007)
26. Floryan, J.M.: Flow management using natural instabilities. Arch. Mech. **58**, 575–596 (2006)
27. Wu, J.Z., Ma, H.Y., Zhou, M.D.: Vorticity and Vortex Dynamics. Springer, Berlin (2006)